HIGH TEMPERATURE EROSION WEAR OF SiC-TaC CERAMIC COMPOSITES

A DISSERTATION

Submitted in partial fulfilment of the

requirements for the award of the degree

of

MASTER OF TECHNOLOGY

in

METALLURGICAL AND MATERIALS ENGINEERING

(With Specialization in Materials Engineering)

by

KAPIL

DEPARTMENT OF METALLURGICAL AND MATERIALS ENGINEERING

INDIAN INSTITUTE OF TECHNOLOGY ROORKEE

ROORKEE – 247667 (INDIA)

MAY, 2016

CANDIDATE'S DECLARATION

I hereby declare that the work presented in this dissertation entitled **High temperature Erosion Wear of SiC-TaC ceramic composites** in partial fulfilment of the requirement for the award of the degree of **Masters of Technology** in **Metallurgical and Materials Engineering** with specialization in **Materials Engineering,** submitted in the **Department of Metallurgical and Materials Engineering, Indian Institute of Technology, Roorkee** is an authentic record of my own work carried out during the period from July 2015 to May 2016 under the supervision of **Dr. B.V. Manoj Kumar,** Associate Professor, Department of Metallurgical and Materials Engineering, Indian Institute of Technology, Roorkee.

The matter presented in this dissertation has not been submitted by me for the award of any other degree.

Dated: **(KAPIL)**

Place: Roorkee **14545007**

CERTIFICATE

This is to certify that above statement made by the candidate is correct to the best of my knowledge and belief.

Dr. B.V. Manoj Kumar

Associate Professor

MMED, IIT Roorkee

ACKNOWLEDGMENTS

I would like to thanks the almighty God for his protection and giving me peace throughout my work. I am highly indebted to **Dr. B.V. Manoj Kumar,** Associate Professor, Department of Metallurgical and Materials Engineering, Indian Institute of Technology Roorkee, for encouraging me to undertake this dissertation as well as providing me all the necessary guidance and inspirational support throughout this dissertation work. He has displayed unique tolerance and understanding at every step of progress. It is my proud privilege to have carried out this dissertation work under his able guidance.

I wish to express my sincere thanks to **Dr. Anjan Sil,** Professor and Head of the Department, Metallurgical and Materials Engineering Department, Indian Institute of Technology Roorkee, for his help to carry out this dissertation.

I would also like to sincere thanks to **Dr. S.R. Meka,** Assistant Professor, Department of Metallurgical and Materials Engineering, Indian Institute of Technology Roorkee, for providing valuable suggestions in X-ray diffraction analysis.

I also like to express my gratitude to Mr. Sandan Kumar Sharma, Dr. Ashish Selokar Mr. Vikas Verma and Mr. Yashpal, Research Scholar for their innumerable discussion, his generosity and willingness to share his knowledge. I sincerely appreciate his valuable persistent encouragement in making this work.

Special thanks to technical staff of Spark Plasma Sintering Lab, Erosion Testing Lab, Metallography Lab, Fabrication Lab, Mr. Sharma and others for their valuable supports, guidance and co-operations to carry out this dissertation work.

I would also like to express my special thanks to Mr. Abhishek Gupta, Mr. Dinesh Singh, Mr. Rakesh Ahlawat, Mr. Niranjan Kumar for their scientific, financial and moral help, inspiration, and valuable suggestions throughout the tenure. Last but not the least I would like to thanks my parents and my brother who have been a constant source of my inspiration to me.

(KAPIL)

ABSTRACT

Highly densified SiC composites were prepared with 10, 20 or 30 wt% TaC addition by spark plasma sintering of SiC and TaC powders at 1800°C at 55 MPa for 5min in Ar atmosphere. The sintered ceramic composites were subjected to erosion by a stream of silicon carbide particles (45-75 μm particle size) impinging at normal angle of incidence at a mass flow rate of 3 g/min and impact velocity of 50m/s at ambient and 400°C using a high temperature erosion tester. Microstructures of the sintered composites consisted mostly of equiaxed grains. Fracture surfaces show mixed mode of fracture, with the large extent of transgranular fracture observed in SiC ceramics containing 10 wt% TaC. With increase in TaC content, micro hardness decreased from 26 to 23 GPa and fracture toughness slightly increased from 3.48 to 3.85 MPa.$m^{1/2}$. Eroded surface of the composites showed fracture, and pull-out of SiC grains and TaC particles. Erosion rate of the composites varied from 53 mm^3/kg to 166 mm^3/kg for 90°, with minimum erosion rate observed for SiC ceramics containing 30 wt% TaC.

CONTENTS

LIST OF FIGURES

LIST OF TABLES

LIST OF ABBREVIATIONS

SPS - Spark plasma sintering

SEM - Scanning electron microscopy

XRD - X-ray diffractometer

EDX - Energy dispersive X-ray spectroscopy

TGA - Thermogravimetry analysis

DSC - Differential scanning calorimetry

ST10 - SiC with 10 wt. % TaC

ST20 - SiC with 20 wt. % TaC

ST30 - SiC with 30 wt. % TaC

CHAPTER 1
INTRODUCTION

Among structural ceramics, silicon carbide is preferred for cutting tools, ball bearings, seals, sleeves, cylinder liners, dies, and heat exchanger tubes. This is due to the unique combination of high stiffness, strength, high hardness and resistance to wear or corrosion [1-3]. The tribological potential for SiC ceramics has been considerably studied in sliding or erosion conditions.

In sliding conditions, the wear rates vary in the order of 10^{-7} - 10^{-5} mm^3/N-m and coefficient of friction (COF) from 0.2 to 0.8, while [4-7]. The behaviour of SiC ceramics is complicated and mechanisms such as ploughing, deformation, fracture, tribochemical wear are used to assess the extent of damage [4-11]. The effect of sliding, environment or material chemistry are studied for SiC ceramics, whereas the microstructural influence on wear properties is not considerably understood. Cho et al. [10] and Lopez et al. [11-13] reported decrease in wear resistance when sliding load, grain coarsening or intergranular phase content are increased in paraffin oil lubricated sliding tests. Kumar et al. [14] recently identified superior wear resistance for the SiC ceramics prepared with small amount (3 wt%) of AlN-SC_2O_3 additives that consists of duplex microstructure of elongated and fine equi-axed grains with clean grain boundary. The microstructural features were found to affect the erosion wear of SiC ceramics significantly [15-17]. Erosion causes major loss of material in several structural applications for example cutting tools, burner parts and parts of gas turbine and several other parts. The solid particle erosion of SiC ceramics and SiC-TiB_2 composites is reported to exhibit anomalous angle or particle size dependence [18, 19]. While brittle fracture occurs via lateral cracking, the contribution of plasticity is also reported to be significant for the erosion of SiC ceramics and their composites [15, 19, 20].

In order to further improve resistance against wear, new ceramic materials with desired combination of properties are to be developed for their extended use in structural applications. Among other approaches, addition of proper material is a

promising one to achieve considerable improvement in properties of SiC ceramics. For instance, Si_3N_4 [21] addition increases strength, and TiC [22] or TiB_2 [19] addition improves fracture toughness of SiC ceramics. In this regard, the incorporation of TaC in SiC can be attractive. It is well known that SiC has higher hardness (2700 kg/mm^2) and oxidation resistance, whereas TaC has high elastic modulus (480 GPa) and high temperature strength [23]. Thus, the composite of SiC-TaC is expected to exhibit improved properties in wear conditions. However, processing and characterization of SiC-TaC composites is difficult and hardly reported.

Yongdong et al. [24] prepared C/SiC–TaC composites by powder infiltration (PI) combined with chemical vapor infiltration. During ablation testing using oxyacetylene torch, TaC oxidized to Ta_2O_5 and the liquid obstructed the diffusing ablative flame channels by filling pores, cracks or interspaces in the matrix.

Sintering of ceramics is generally difficult due to strong covalent or ionic bonding, high melting points and low diffusion coefficient. Silicon carbide ceramics are liquid-phase sintered using variety of sintering additives: Al-B-C, oxides, AlN-oxides to obtain engineered microstructure and improved mechanical properties [25-29]. Spark Plasma Sintering (SPS) is an effective consolidation technique for metallic or ceramic powders at lower temperature and shorter times. SPS is a pressure sintering technique which is based on the high temperature plasma generated by the discharge phenomenon known as electric spark. A low voltage and high energy pulsed current produces spark plasma in the gap between powder particles at high temperatures. The large current produces Spark Plasma: Evaporation and melting of powders; Spark Impact Pressure: Eleminates the impurities and adsorptive gas of powder particles which is on the surface; Joule heating: Local high temperature is generated momentarily which is about several to ten thousands degree centigrade; Electrical field diffusion: high speed diffusion takes place which is occured due to the high speed of moving of ions. SPS has been attractive because of short sintering duration (few minutes) compared to long duration (hours) in conventional sintering. The other advantage in SPS is the less temperatures (usually 200-300°C less than conventional sintering) required for densification [30, 31]. Commercially available Ta and TaC were used to prepare 96% dense tantalum carbide ($TaC_{0.9}$) by SPS at 1400°C for 5 min. The microstructure consisted of equiaxed grains and the ceramic showed a

maximum flexural strength of 498 MPa [32]. In other work, the addition of at least 20 vol% SiC was found effective in eliminating closed pores to yield full density by SPS at 1800^0C for 5 min. TaC grain size decreased with increase in SiC concentration. The TaC- 40 vol.% SiC composite exhibited the maximum highest flexure strength of 703 MPa and maximum fracture toughness of 6.8 MPa $m^{1/2}$ [33].

SiC ceramics are generally sintered at around 2200°C for a holding time of 2-3 hours in conventional sintering, while in spark plasma sintering, SiC ceramics can be sintered at temperatures less than 2000°C for a holding time of 10-15 minutes [30] . It was reported that the addition of small amount of sintering additives results in improved sinterability and strength of SiC ceramics [34].

To the best of my knowledge, tribological properties of SiC-TaC composites have not been investigated. In this context, SiC composites with TaC: 10 to 30 wt% were prepared via spark plasma sintering. Owing to the expected use of these novel composites in applications like ball bearings, nozzles, heat exchanger tubes, etc. their performance potential under erosion wear conditions will be systematically investigated.

The major aim / objectives are the following:

1. To fabrication of dense SiC-TaC composites (10, 20 or 30 wt%) by spark plasma sintering
2. To study solid particle erosion of the SiC-TaC composites at ambient to high temperature erosion conditions
3. To understand dominant mechanisms of material removal in erosive wear conditions as function of TaC content.

The above objectives are envisaged by systematic experimental work and analysis of results. The following explains arrangement of various topics of the thesis.

Chapter 2 deals with review of recent research on sintering of SiC ceramics and its composites. The other part of the chapter also deals with the erosion behaviour of SiC ceramics and composites.

The experimental work consisting of spark plasma sintering of SiC-TaC composites and details of SiC particle erosion in ambient and high temperature conditions are explained in **Chapter 3**.

The results obtained in sintering and erosion testing are provided in **Chapter 4**. A detailed discussion of the experimental results and characterisation are also provided.

The major conclusions obtained from the thesis work and scope for the future work is highlighted in **Chapter 5**.

CHAPTER 2

LITERATURE REVIEW

2.1 SiC Ceramic

The crystal structure of SiC is tetrahedral having strong bonds of carbon and silicon atoms. SiC is unreactive to acidic and alkaline salts up to 800°C [35]. SiC unique properties of low density, high hardness, high strength, high thermal conductivity, abrasion resistance, and resistance to corrosion makes it suitable for tiles; pump parts and refractory bricks, for heat exchangers in power generation and as armour material in military sector.

2.2 Chemical Bonding and Crystal structure

Silicon carbide is a lightweight covalently bonded ceramic having strong covalent and ionic bond. 3.210 g/cm^3 and 3.208 g/cm^3 are the theoretical density of β-SiC and α-SiC (6H polytype) respectively. 3C, 4H, 6H, 15R and 9T are the SiC polytypes crystal structures where for cubic (C), hexagonal (H), rhomohedral (R) and tetrahedron (T). Zinc blend and wurtzite structure are found for β-SiC and α-SiC.

Fig. 2.1 shows zinc blend and wurtzite structure of SiC. β-SiC to α-SiC transformation takes place on heating SiC. Above 2000°C undoped β-SiC transforms to 6H and 15R in which 15 R is a metastable phase. Generally β-SiC is formed as zinc blend structure at temperature less than 1700°C. At a temperature more than 1700°C, α-SiC is formed as hexagonal structure. [36]

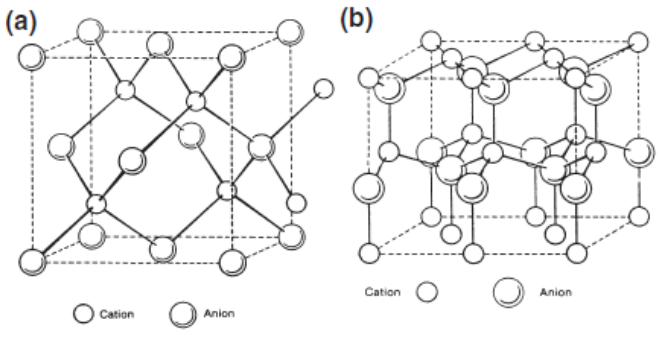

Fig. 2.1 SiC Crystal Structures: (a) Zinc blend structure for β-SiC and (b) wurtzite structure for 6H α-SiC [36].

2.3 Properties of silicon carbide:

Silicon carbide has superior properties like low density, high strength, low coefficient of thermal expansion, high hardness, high thermal conductivity, high elastic modulus and excellent thermal shock resistance. The various properties of silicon carbide are given in **Table 2.1**[37]

Table 2.1. Properties of silicon carbide ceramics [37]

Physical	**Units**	**SI/Metric**
Density	g/cc	3.21
Hardness	Kg/mm^2	2800
Compressive Strength	MPa	3900
Elastic Modulus	GPa	410
Flexural Strength	MPa	550
Fracture Toughness K_{IC}	$MPam^{1/2}$	4.6
Poisson`s Ratio	-	0.14
Melting Point	°C	2780
Maximum Use Temperature (No Load)	°C	1650
Thermal Conductivity	W/m-K	120
Coefficient of Thermal Expansion	10^{-6}/°C	4.0
Specific Heat	J/Kg-K	750
Volume Resistivity	Ohm*cm	10^2-10^6

2.4 Applications of silicon carbide

Silicon carbide has wide range of applications due to its good properties. Typical uses of SiC included abrasives, refractories, ceramics, and numerous high-performance components. Structural and wear applications are constantly developing eg. cutting tools, ball bearings, seals, sleeves, cylinder liners, dies, and heat exchanger tubes.[38]

2.4.1 As Abrasive:

It is widely used as abrasive because of its hardness and low cost. It is used on grinders, emery papers and as abrasive material in water jet cutting and wear testing.

2.4.2 Ball bearings and Seal-ring

Silicon Carbide is also used in ball bearings and seal rings due to its combination of favourable properties like high hardness, high elastic modulus and low density, low coefficient of thermal expansion, higher chemical corrosion resistance especially for high speed bearings.

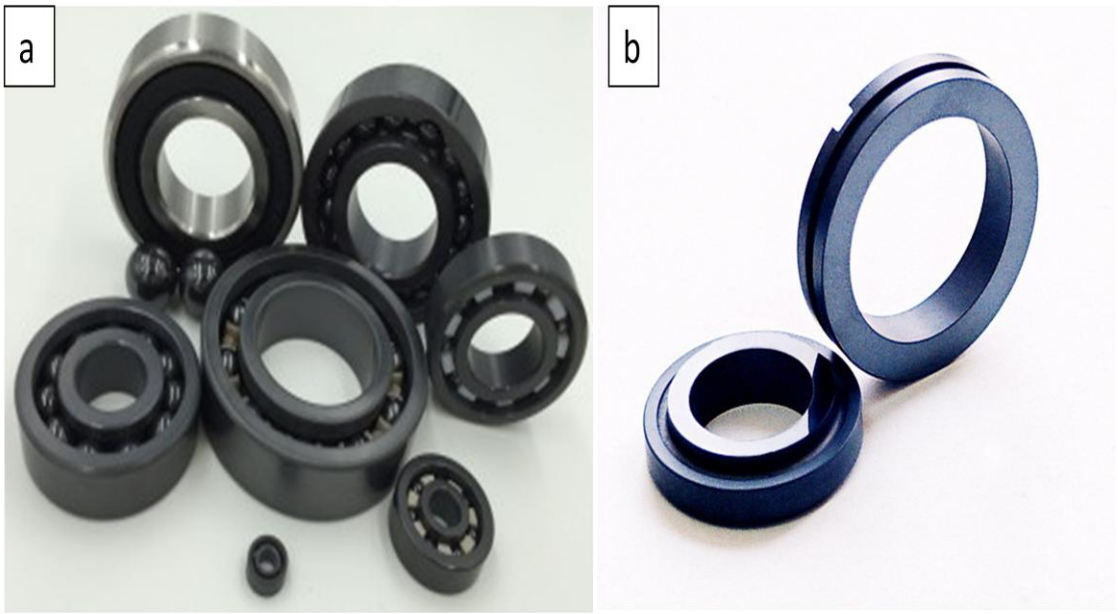

Fig. 2.2 (a) Ball bearing (b) Seal-ring [39].

2.4.3 Cutting-Tool Application

SiC combined with other carbide combination found suitable for cutting-tools as they have high hardness, high strength, and high wear resistance. **Fig.2.3 a. and 2.3 b** shows the Al_2O_3-SiCw and steel cutting-tools respectively. These are cost effective for difficult-to-machine metals. For turbines in aerospace applications Ni-based super alloys are preferred.

Fig. 2.3 Applications of Al_2O_3-SiC_w composites: (a) cutting-tool inserts, (b) insert (marked with arrow) machining hardened tool steel [38].

2.4.4 As constructional material:

Silicon carbide has many applications in defence. Many components like bullet proof vests (Fig. 2.4), Cobham armour which is used to protect main battle tanks and dragon skin are prepared by using silicon carbide. [39]

Fig. 2.4 Bullet proof vests [39].

Silicon carbide is widely used in automobiles. Automobile parts like brakes and clutches plates (Fig. 2.5) and diesel filters.

Fig. 2.5 Disc brake and clutch plate made of silicon carbide [39].

2.4.5 Biomedical applications of SiC

Silicon carbides processed materials are used in biomedical applications as in membranes, stents, orthopaedic implant etc [38].

2.5 SiC ceramics and their composites

2.5.1 Effect of Si_3N_4

Yeom et al. [40] studied the properties of SiC-Si_3N_4 composites sintered with yttria and Scandia. They have found that the fracture toughness increased while thermal conductivity decreased with increasing silicon nitride content from 0 to 35 vol. %.

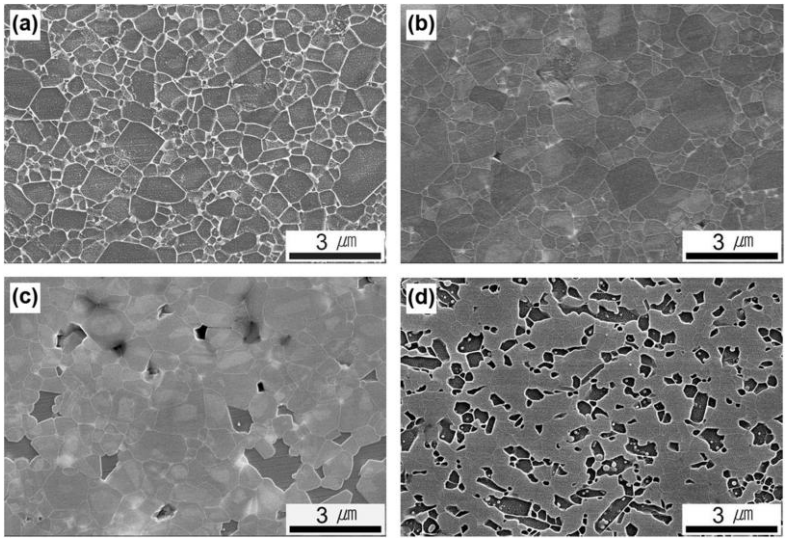

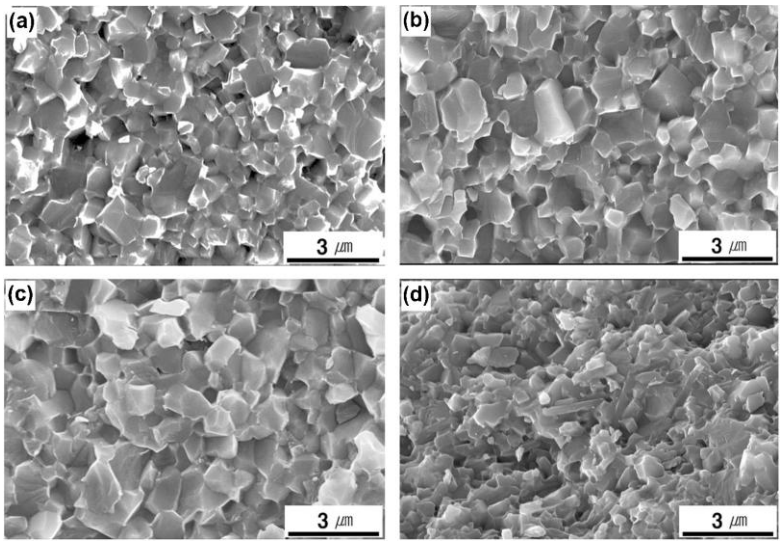

Fig. 2.6 Typical microstructures of monolithic SiC and SiC–Si_3N_4 composites sintered with 2 vol% Y_2O_3–Sc_2O_3: (a) SiC, (b) SiC-1 vol% Si_3N_4 (c) SiC-10 vol% Si_3N_4, and (d) SiC-35 vol% Si_3N_4 [39].

Also they found that electrical resistivity also decreased with increasing silicon nitride content from 0 to 10vol. %. They have added the yttria and Scandia for increasing electrical conductivity by making effective doping of nitrogen in SiC grains.

2.5.2 Effect of Alumina

Unlu et al. [34] reported the effect of alumina on the spark plasma sintering of SiC ceramics. SiC ceramics were prepared with the addition of alumina as sintering additive by spark plasma sintering at different temperatures 1700-1800°C applying 40 and 80 MPa pressure. The effect of alumina, temperature and pressure on the mechanical properties and densification behaviour was observed. They have found that with the increase in temperature and pressure leads to increase in relative density, hardness and fracture toughness. The addition of 5 vol. % Al_2O_3 shows that the relative density increased from 87.2% to 97.7% and hardness increased from 10.2 to 26.8 GPa. The fracture toughness was also higher for 5 vol. % addition Al_2O_3.

Table 2.2. Relative density, Vickers hardness and fracture toughness values of the SiC ceramics with Al_2O_3

Samples	SPS parameters [°C, MPa, min.]	Relative density [%]	Vickers hardness [GPa]	Fracture toughness [MPa*$m^{1/2}$]
SiC+5vol.% Al_2O_3	1700, 40, 5	97.7	26.4	4.6 ± 0.2
	1800, 40 ,5	97.8	26.9	5.8 ± 0.5
	1700, 80, 5	97.5	26.2	5.7 ± 0.2
	1800, 80, 5	98.3	28.9	5.9 ± 0.2
Monolithic SiC	1800, 40, 5	87.2	10.2	-
	1950, 80, 5	99.7	31.9	3.6 ± 0.3

2.5.3 Effect of AlN

Zhang et al. [41] studied the effect of AlN on thermal conductivity of SiC ceramics. They have prepared SiC ceramics with 0.5-10 vol. % additions with two step sintering, B_4C and C as additives. They have investigated that thermal conductivity decreased with increasing AlN content. Thermal conductivity is decreased due to the point defect scattering by the difference in inter atomic forces and the size of atoms.

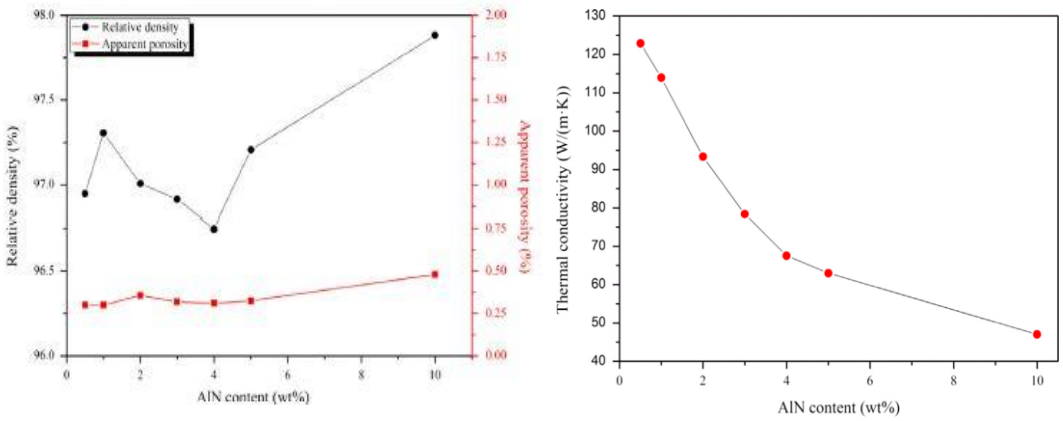

Fig. 2.7 Effect of AlN content on (a) Relative density and apparent porosity, (b) thermal conductivity in SiC ceramics [40].

When AlN was added in the SiC ceramics, exist two situations:

(1) Al and N atoms diffuse into the host lattice and replace C and Si atoms respectively.

(2) AlN exists as a secondary phase in SiC ceramics. These two effects lead to the reduced of thermal conductivity.

2.5.4 Effect of h-BN addition

Motealleh et al. [42] investigated the effect of flaky hexagonal (*h*) BN additions (1, 5, and 10 vol.%) on the sliding-wear behaviour of sintered SiC composites which are made by spark-plasma sintering. They found that hardness is decreased due to that h-BN is softer than SiC while fracture toughness improved with the addition of h-BN content.

2.5.5 Effect of Boron carbide in SiC composites

Maître et al. [43] have found that free boron plus free carbon additions in SiC leads to higher densification with absence of any abnormal grain growth. It is also seen that pure SiC density is not marginally increased with addition of boron carbide processed via SPS.

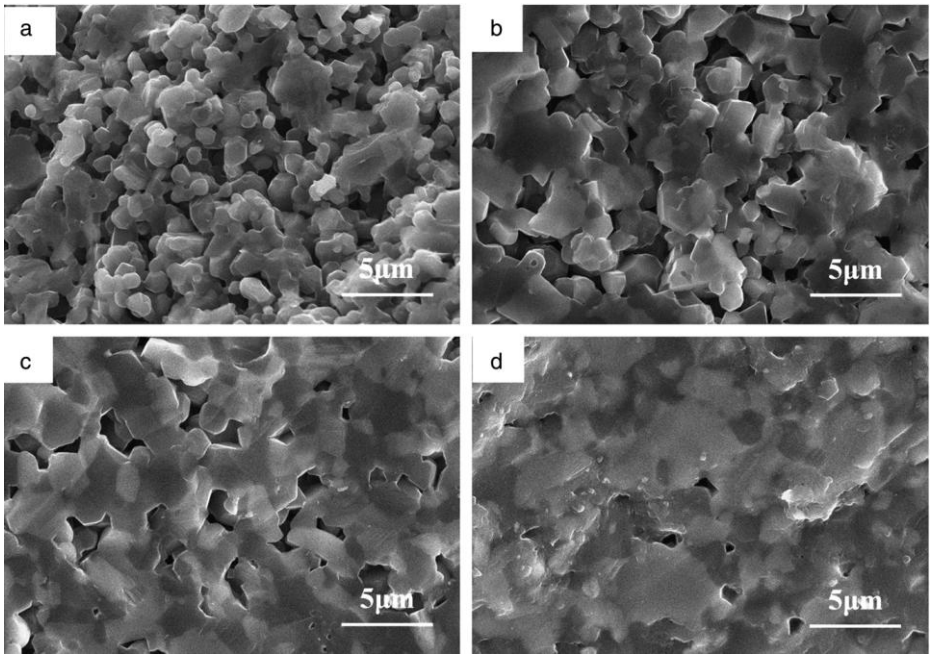

Fig. 2.8 SEM micrographs of fracture surface of SiC ceramics with addition of B_4C as additive : (a) sintered at 1800 °C; (b) sintered at 1850 °C; (c) sintered at 1900 °C; and (d) sintered at 1950 °C [43].

Formation of a borosilicate vitreous phase is observed in TEM. Free carbon and free boron addition in SiC processed at 1950 ◦C for 5 min. at 100 MPa results densified material [44]. With high B_4C content in SiC increases fracture toughness and flexural strength. Borosilicate liquid phase form during sintering with B_4C dissolution.

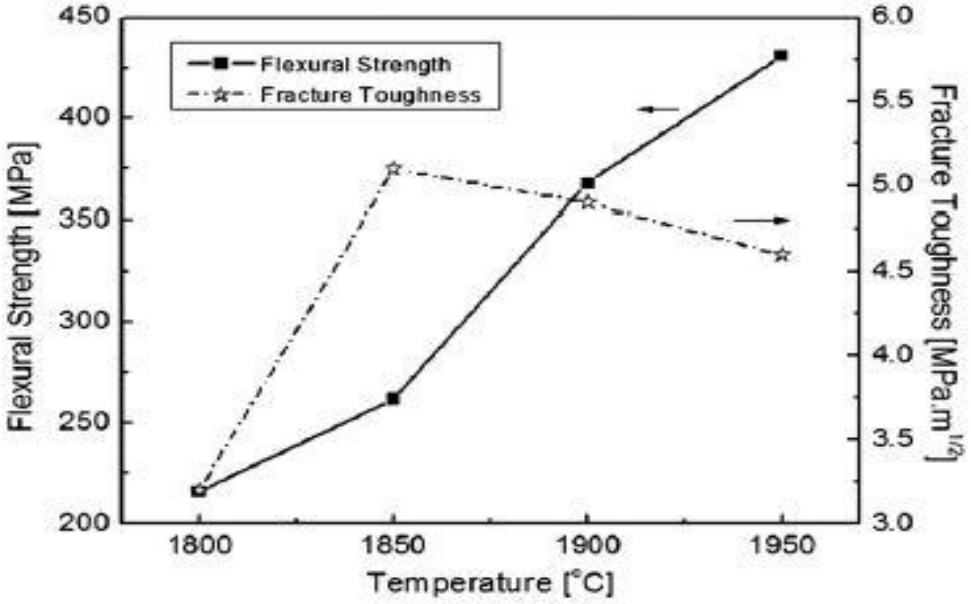

Fig. 2.9 Flexural strength and fracture toughness of the SiC ceramics with B_4C additive sintered at different temperature [43].

2.5.6 Effect of ZrB_2

Krupa et al. [45] have studied the effect of ZrB_2 addition on the properties of SiC composites. They have prepared the SiC composites with the addition of 10, 20 and 30vol% ZrB_2 to observe the various properties of composites and machinability of SiC composites by EDM. Highly densified SiC composites were produced by hot pressing at 1900°C.The density of composites decreased with the increase ZrB_2 content due to high covalence and coarser particles than SiC particles. It was found that with the increasing content of ZrB_2 hardness of composites increased while electrical resistivity and flexural strength is reduced.

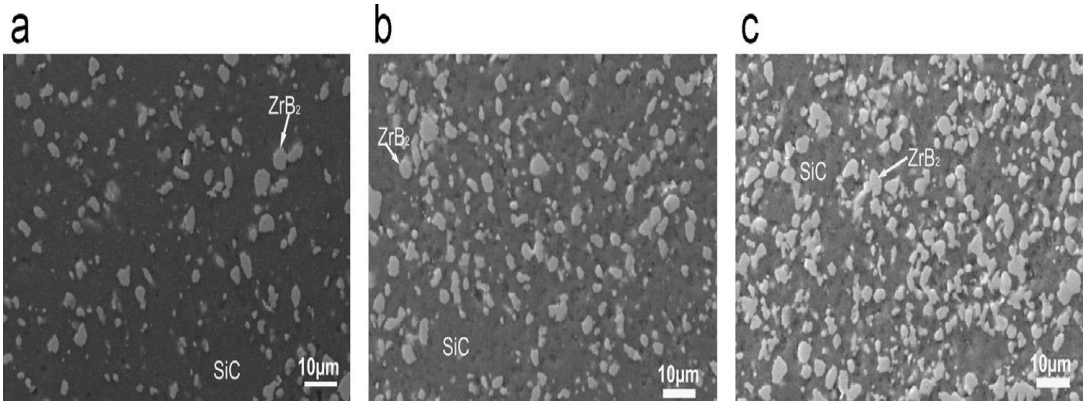

Fig. 2.10 Scanning electron micrographs of SiC-ZrB_2 composites (a) 10 vol. % ZrB_2 (b) 20vol. % ZrB_2 (c) 30vol. % ZrB_2 [45].

2.5.7 Effect of TiC

Luo et al. [46] have been evaluated the properties of SiC-TiC composites made by SPS at 1800°C. The relative density of SiC-TiC composites is close to theoretical density with addition of 30% TiC content. The fracture toughness and strength are maximum when the amount of addition TiC content is 30%.

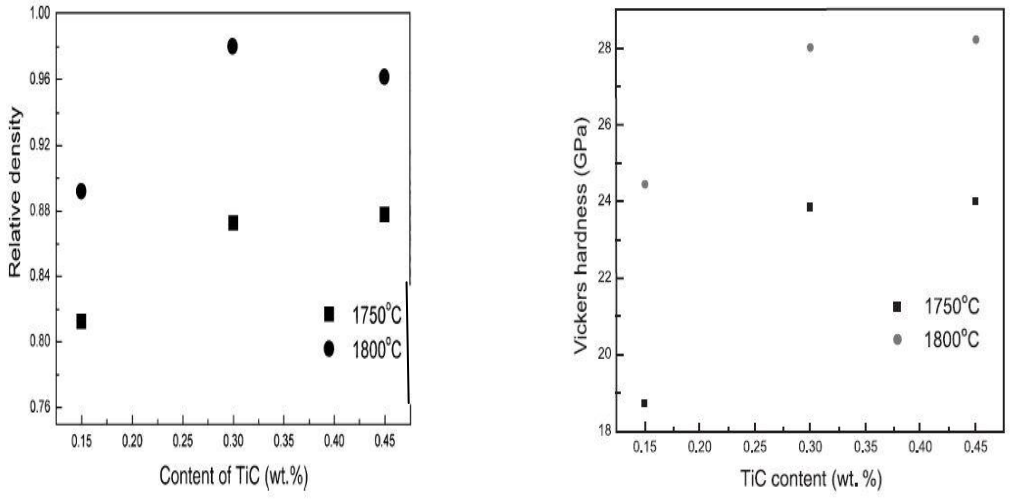

Fig. 2.11 Relative density and Vickers hardness as a function of TiC content in SiC-TiC composite [46].

Fig.2.12 showed the value of fracture toughness (K_{IC}) of SiC–TiC composites and maximum value of K_{ICmax} = 6.2±0.6 MPa $m^{1/2}$ when TiC content rises to 30%, which is almost double as compared to pure SiC ceramic.

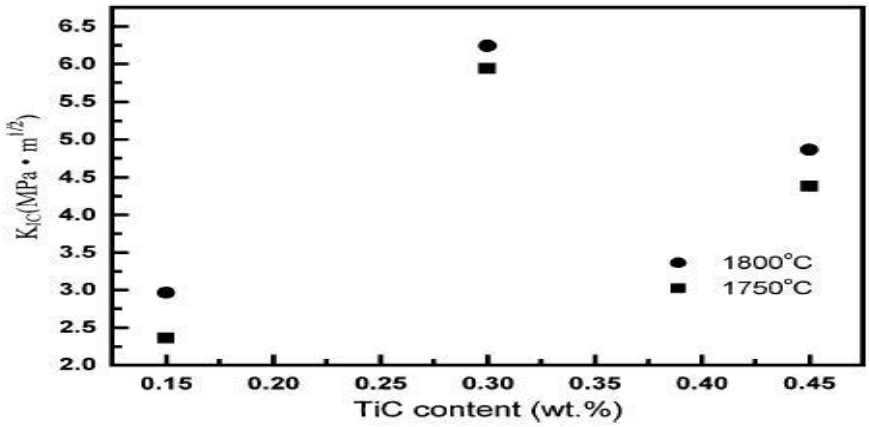

Fig. 2.12 The relationship of fracture toughness and TiC content of SiC-TiC composite [46].

Fig. 2.13 shows the SEM images of the fracture surface of composites with 30% TiC content, which were fabricated 1750 and 1800 °C. Fig. 2.13 (a) show the fracture surface fabricated at 1750 °C, existed more pores and fracture surface covered with fused phases. With the increasing temperature from 1750°C to 1800 °C, the pores decreased in composites. Bending strength was improved due to the transgranular fracture of SiC grains while fracture toughness was increased due to the intergranular fracture of TiC grains.

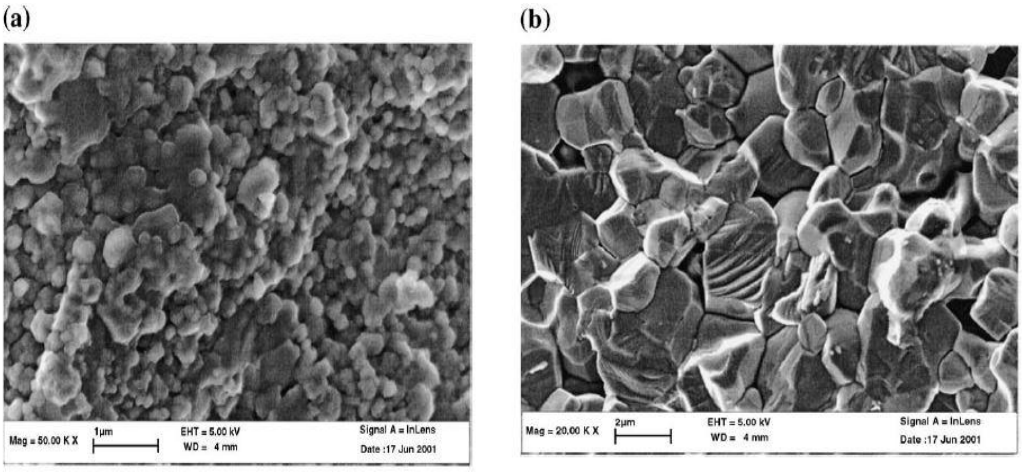

Fig. 2.13 SEM micrographs of the fracture surface of SiC-TiC composites: (a) 1750 °C, (b) 1800 °C [46].

2.5.8 Effect of WC

Sharma et al. [47] observed the effect of WC content on the properties of SiC composites. They prepared the SiC composites with the addition of 0, 10, 30 and 50 wt. % WC content by hot pressing. It was observed that fracture toughness is max for 50 wt. % WC content addition in SiC ceramics, while the hardness is max when the addition of WC content is 30 wt %.

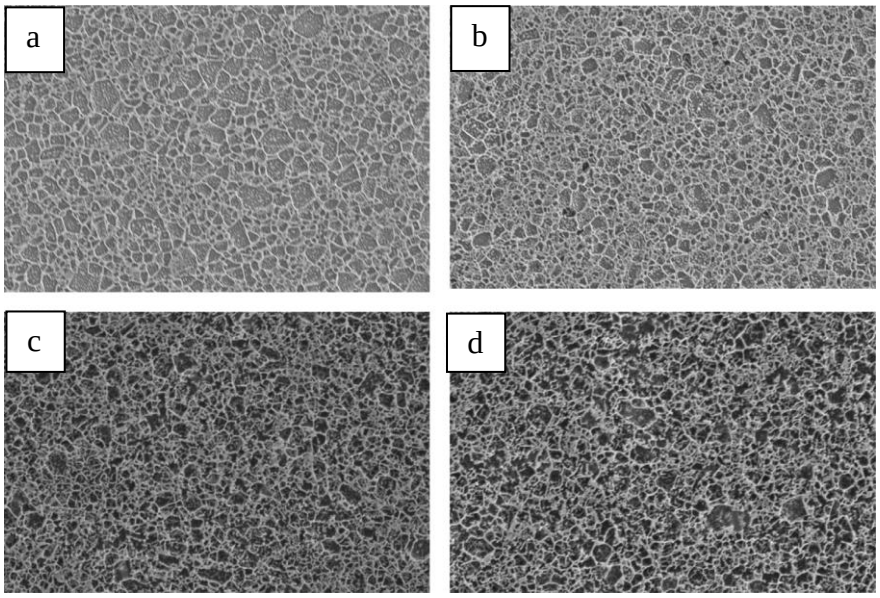

Fig. 2.14 BSE images of SiC ceramics with addition of (a) 0% WC, (b) 10% WC, (c) 30% WC, (d) 50% WC [47].

A maximum fracture toughness of 6.7MPam$^{1/2}$ was observed for SiC ceramics with 50 wt%WC, whereas a high hardness of 26 GPa obtained for SiC ceramics with 30 wt%WC.

Table 2.3. Mechanical properties of SiC –WC composites. [47]

Sample	Volume fraction	Hardness (GPa)	Fracture toughness (MPa*m$^{1/2}$)
0 wt.% WC	0	23.95 ± 0.97	5.85 ± 0.30
10 wt.% WC	0.08 ± 0.01	24.02 ± 1.12	6.36 ± 0.22
30 wt.% WC	0.28 ± 0.01	26.33± 0.71	6.47 ± 0.13
50 wt.% WC	0.46 ± 0.01	24.26 ± 1.12	6.66 ± 0.12

2.5.9 TaC-SiC composites

Liu et al. [33] studied about the TaC-SiC composites prepared by Spark Plasma Sintering. They prepared TaC-SiC composites with 5 to 40 vol% 6H-SiC content by SPS at a temperature of 1800°C for 5 min. They observed that with the addition of SiC closed porosities eliminated in the last stage to achieve full densified TaC with at least 20 vol% SiC. The grain size of TaC decreased with increase in SiC content. The 40 vol% SiC composition had the highest flexure strength and fracture toughness of 703 MPa and 6.8MPa $m^{1/2}$ due to the addition of the SiC. At a temperature of 1400°C composites with 20 and 40 vol% SiC showed higher flexural strength than room temperature, due to silica rich glassy layer formation by the oxidation of SiC.

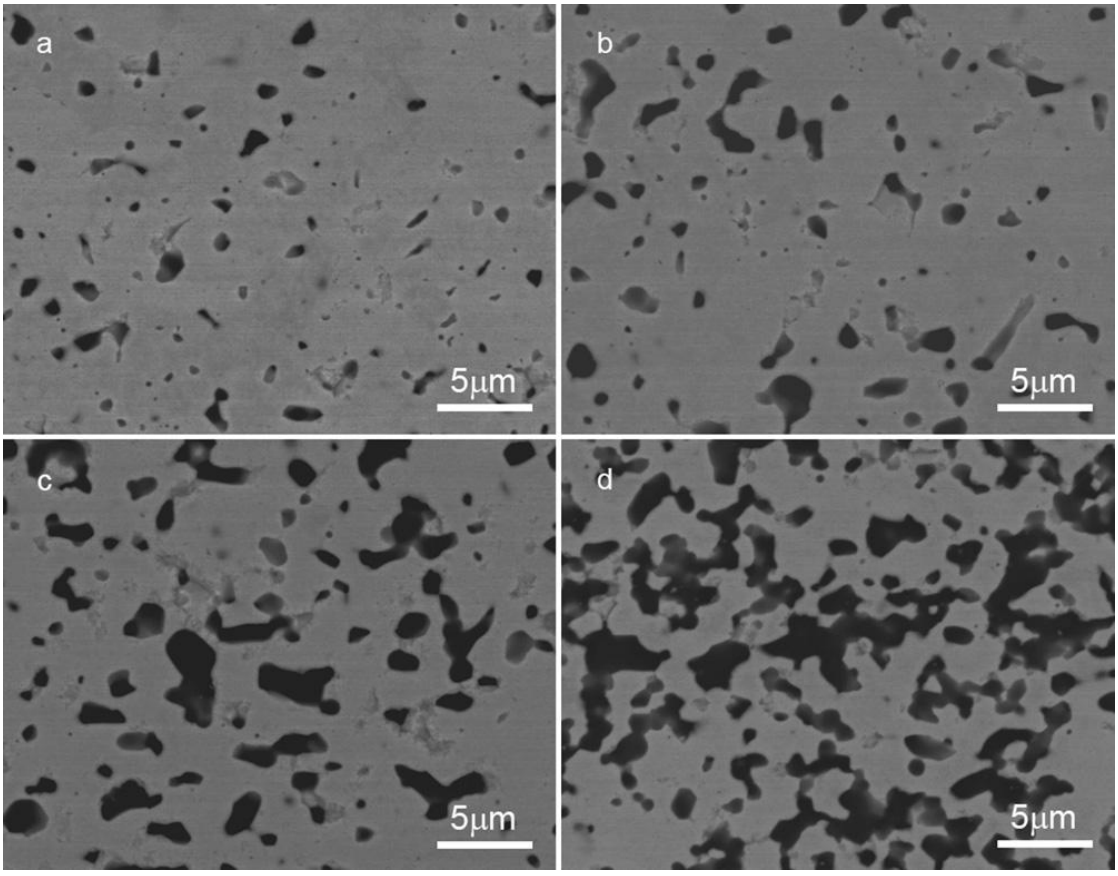

Fig. 2.15 SEM images of the microstructures of the TaC-SiC composites with (a) 5 vol.% SiC; (b) 10 vol.% SiC; (c) 20 vol.% SiC; (d) 40 vol.% SiC.[33]

The TaC-SiC composites with 20 and 40 vol. % SiC additions showed higher flexural strength at 1400 ◦C than room temperature, due to the formation of the silica rich glassy layers as a result of the oxidation of the SiC phase.

Table 2.4. Mechanical properties of the TaC-SiC composites. [33]

Material	Young's modulus (GPa)	Hardness (GPa)	Fracture toughness ($MPam^{1/2}$)
5vol.% SiC	507 ± 11	18.4 ± 0.6	5.3 ± 0.4
10vol.% SiC	518 ± 13	19.1 ± 0.6	5.9 ± 0.7
20vol.% SiC	511 ± 12	19.9 ± 0.7	6.4 ± 0.7
40vol.% SiC	498 ± 10	21.0 ± 0.8	6.8 ± 0.9

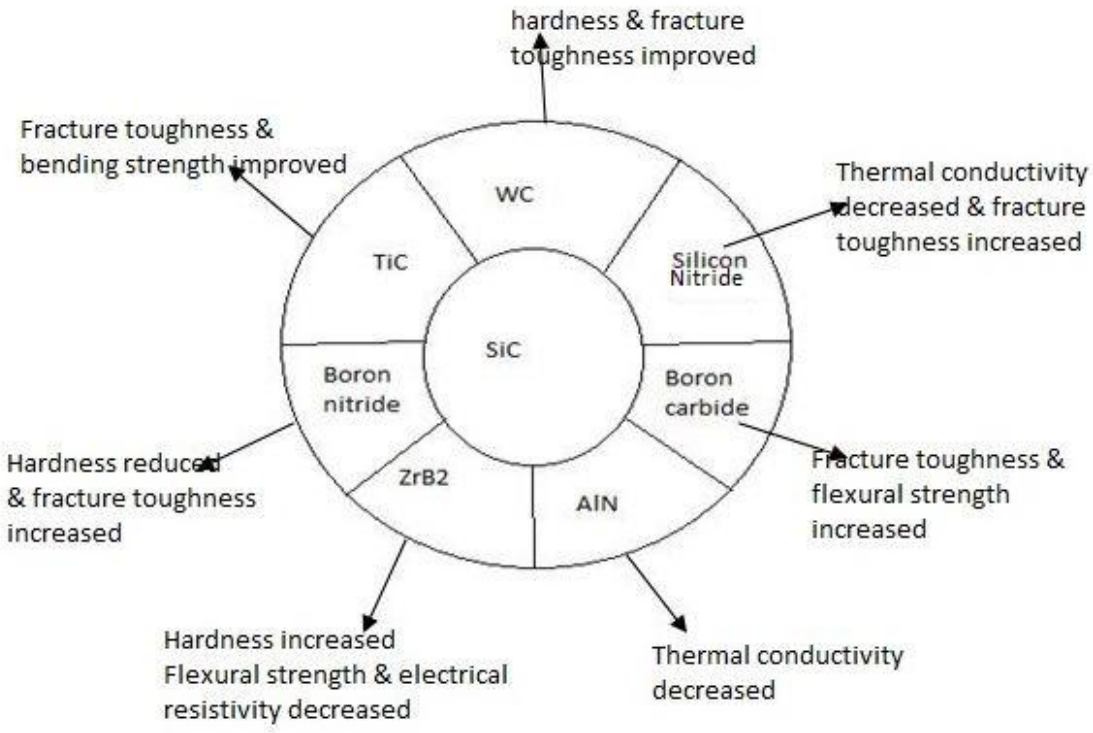

Fig. 2.16 Effect of different ceramic addition on the properties of SiC composites.

2.6 Erosion behaviour of SiC ceramics and their composites

Erosion wear behaviour is influenced by microstructure, mechanical properties and heat treatment of material itself. It also depends on the characteristics of erodent particle and some other factors. As many researchers have done a lot of study in this field, many other also correlate properties of erodent particle with the characteristics of erosion of silicon carbide composites, all the relevant data so far available related to erosion are summarized below.

2.7 Erosion

Erosion is a material removal mechanism, occurred in a number of engineering systems. Erosion may be defined as material removal process from a surface due to the interaction between surface and fluid, or impinging solid or liquid particles. Erosive wear occurred by the impact of solid or liquid particles against the surface.

The particles that are impacting on the surface gradually remove the material from the surface through repeated deformation and cutting conditions. [48] Erosive wear occurs in a wide range of machineries and industries components; for example, damage of gas turbine blades by dust clouds, hydro turbine under water parts etc. The erosive wear rate depends on various factors such as particle shape, hardness, and impingement angle and impact velocity along with characteristics of surface which is being eroded. The impingement angle is one of the important factors. The wear rate is the maximum at an angle of impingement of 30° for ductile materials while for brittle materials wear rate is maximum at 90° angle [49].

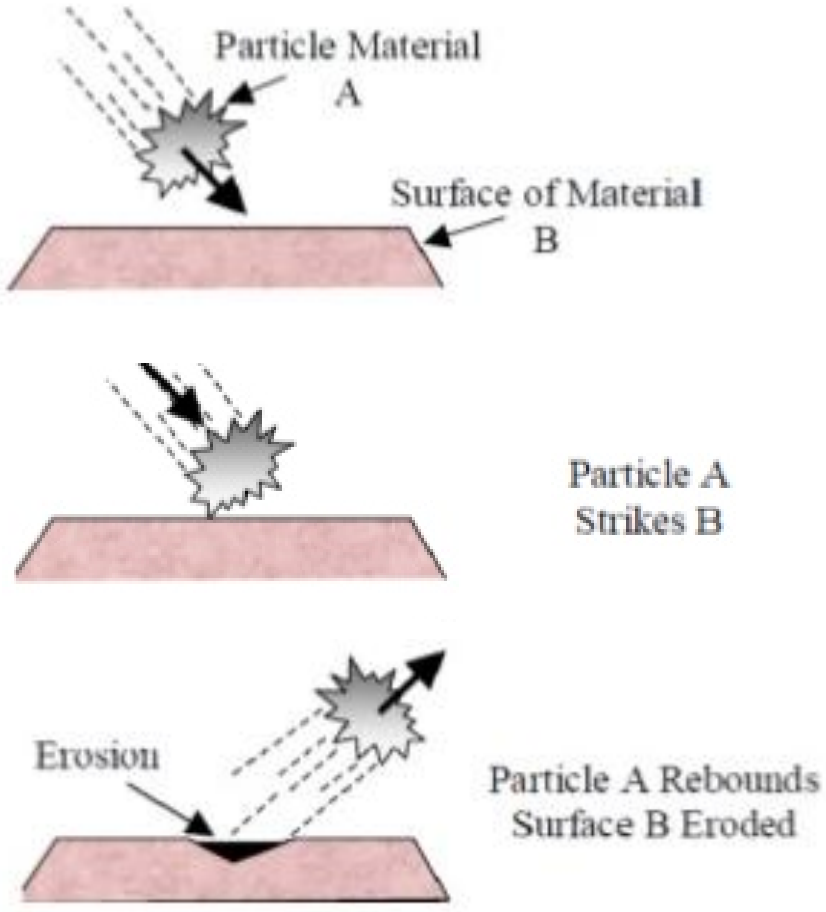

Fig. 2.17 Impingement of solid particles on the surface [50].

2.8 Solid particle erosion

When the solid particles impact on the surface of composites, type of damage occurs: the removal of the material due to repeated deformation and the cutting action. When the solid particle impinges at low angle, it skids on the surface of material and at the same time indentation created. This skid is related to loss of material due to plastic deformation and indentation is related to cutting action. As the velocity of impact reduces, solid particle tend to skid on the surface of material and damage due to cutting is reduced. So at lower velocity of impact, particle does not skid in cutting damage but only plastic deformation damage occurs.

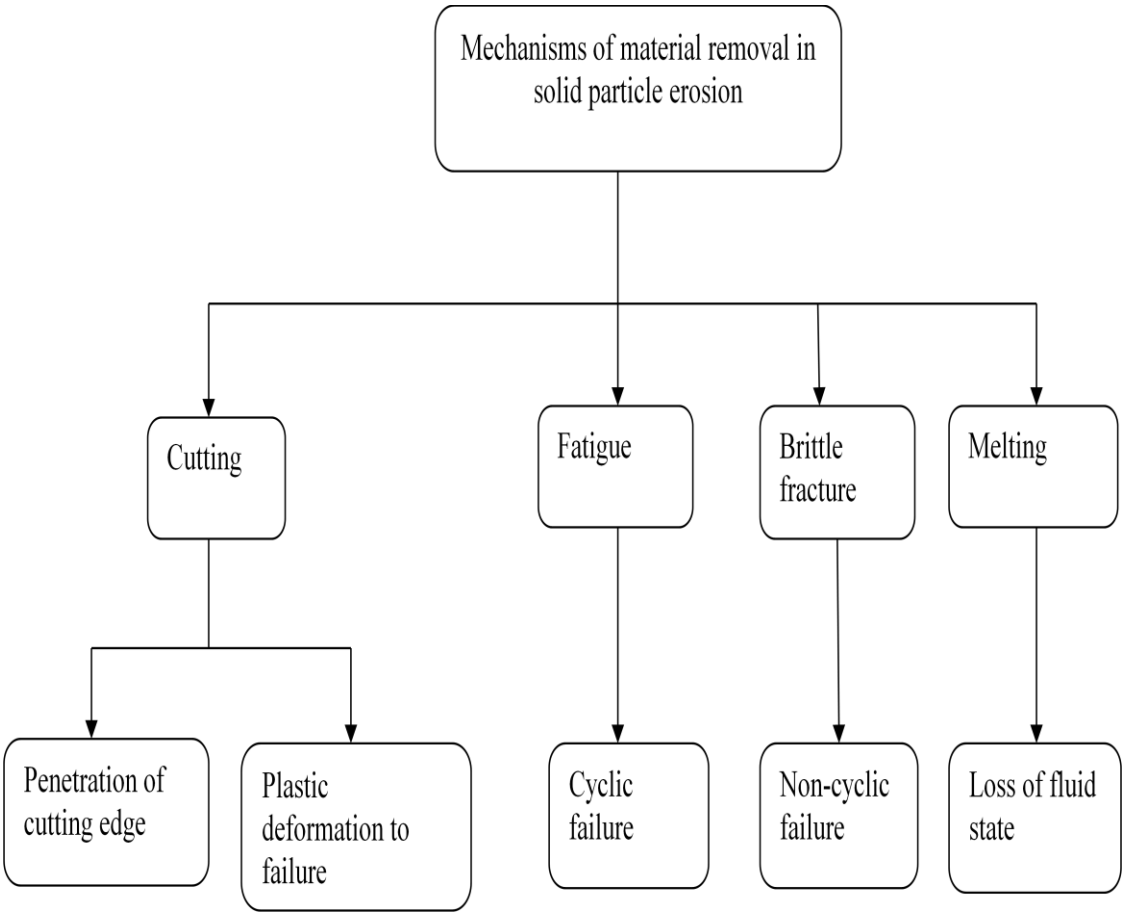

Fig. 2.18 Material removal mechanisms in solid particle erosion [49].

2.9 Factors affecting erosion behaviour

The erosion rate depends on many factors like impact velocity, size of particle and the relative hardness and toughness of the erodent and target for brittle materials. The impact velocity and particle shape of erodent are major factors determining the erosion rate for ductile materials. The erosion rate is increased with increase in the erodent hardness. The erosion rates with hard silicon carbide erodent were > 100 times those caused by the softer silica. This was due to differences in the mechanisms of material removal. Particle size, kinetic energy, toughness and relative hardness of the target and erodent are some factors to determine erosion rate for brittle materials while shape and kinetic energy of the erodent are main factors for erosion o ductile materials. There is no or less effect of hardness and toughness of erodent on erosion rate for ductile materials [51]. The material removal during erosion is dependent on many operating parameters which are as follows:

2.9.1 Impact velocity

Impact velocity of the erodent has significant effect on erosion rate. The erosion rate is generally defined loss of material to the weight of erodent particles. Theories of erosion for brittle materials predict that steady state erosion rate ΔW (weight loss per unit weight of impacted particles) is given by:

$$\Delta W = K V^n D^m \quad \text{.....(1)}$$

where v is the velocity of particle, D is the particle diameter, K is a velocity and size-dependent function of properties of material. n lies in the range 2 to 3. The velocity exponent is also affected by angle of impact and particle size. Goodwin et al. noted that with the decrease in particle size, the velocity exponent decreases. [52]

2.9.2 Particle hardness

Sundararajan [53] studied the effect of hardness of abrasive particles on the erosion rate of target material. They have found that as long as the particle was at least 1.5 times harder than target material, the resulting erosion rate was not depend on hardness of particle. But when the hardness of particle is comparable to target, a significant reduction in erosion was observed.

2.9.3 Particle shape

The influence of shape of particle on the erosion rate has been studied by several investigators. Brown et al [54] and Levy and Chik [55] observed that erosion rate is higher when eroded by angular particles compare to spherical particles.

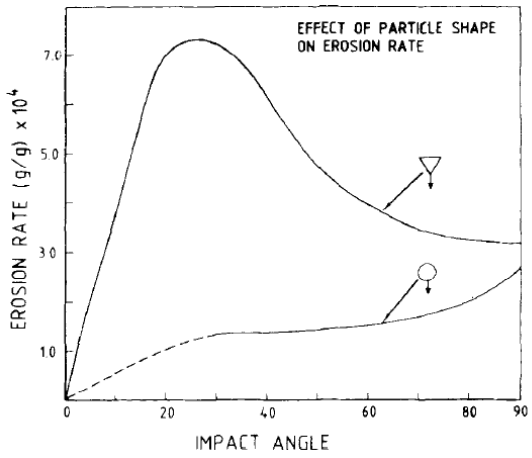

Fig. 2.19 Variation of erosion rate with respect to impact angle with particle shape [54].

It is found that angular particles are more effective compare to spherical particles for erosion. The erosion rate increased with increasing squared perimeter to area ratio ($P^{2/}A$) and decreasing width to length ratio (W/L) for erodent particles. Erosion is the maximum at low impact angle and at high angularity.

2.9.4 Particle size

Particle size of erodent is also an important variable. The effect of particle size has been studied by several workers. Goodwin et al. studied the erosion of steel by quartz particles. The obtained results are shown in **Fig. 2.20** which indicates that when particle size is increased up to a limiting size (50 to 100 microns), erosion increases and after that (more than 100 microns), the erosion rate is independent of particle size. Montgomery and Clark [56] studied the effect of particle size. Since erosion rate decreases with decreasing the size of particles (less than 100 microns), it is quite natural except that below a critical size of particle erosion rate will become negligible.

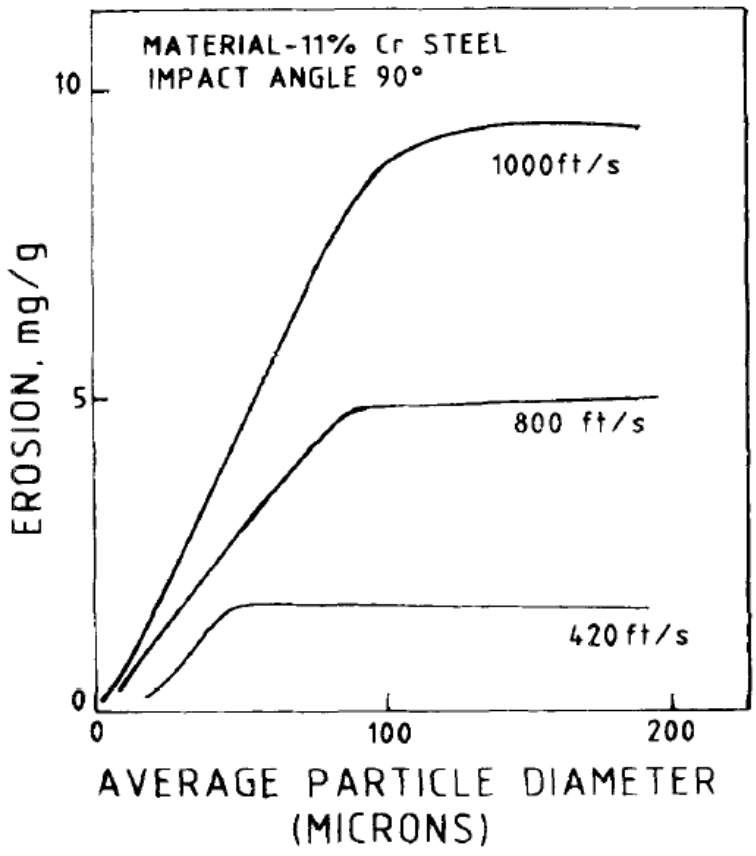

Fig. 2.20 Variation of erosion rate of steel with particle size [56].

2.9.5 Particle concentration

Erosion rate should be independent of particle concentration as long as each particle impact event is equally effective. At higher concentration, where a particle interference effect occurs, the erosion rate decreases [57].

2.9.6 Impact angle

Impact angle is defined as the angle between particle trajectory and the surface of target. The effect of impingement angle on erosion is very much determined by the nature of target material as shown in **Fig. 2.21**. Erosion rate is the maximum at normal incidence angle for brittle materials while for ductile materials erosion rate is the maximum at an impact angle closer to 30°.

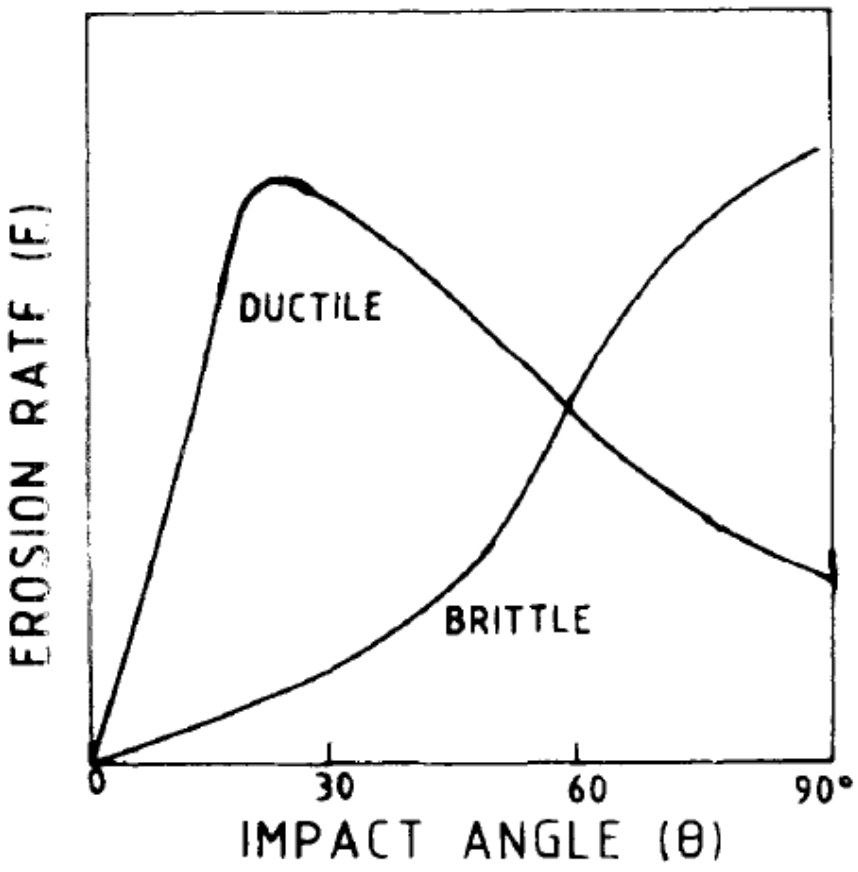

Fig. 2.21 Effect of impact angle on erosion rate in case of Ductile and Brittle Materials [57]

2.9.7 Temperature

Oxidation rate and surface oxide layer thickness and toughness formed at elevated temperatures govern erosion behaviour. It is found by Alman et al. [58] that erosion rate at 700°C is double then that at room temperature in case of WC-Co hard metals. Temperature highly affects the erosion rate [59]. Erosion angle changes from 90° at 23°C to 45° at 1000°C, in sintered alumina. The effect of temperature on erosion is significant above 400 °C which further increases at high temperature. The erosion rate at 800 °C is 1.7 - 2.2 times that at room temperature [60].

2.10 Erosion of SiC ceramics and their composites

Generally erosion is preceded by indentation-induced fracture mechanism, if particles are harder than target material. If the particles are softer than target material, erosion occurs by chipping mechanism. Extensive research has been done to understand the erosion behaviour of SiC ceramics and their composites. Generally, solid particle erosion of SiC ceramics occurs by brittle fracture as a result of radial and lateral cracking [61, 62].

2.10.1 Erosion of reaction bonded SiC

Routbort et al. [15] studied eroded surfaces of SiC composites with different sizes of erodent particles. The erosion wear is reported to not be in agreement with predicted erosion wear rates because of the microstructural effects. They investigated the impact erosion of reaction bonded SiC by angular Al_2O_3 particles (23-270 μm) at room temperature with 54-151 m/s and 10-90°.

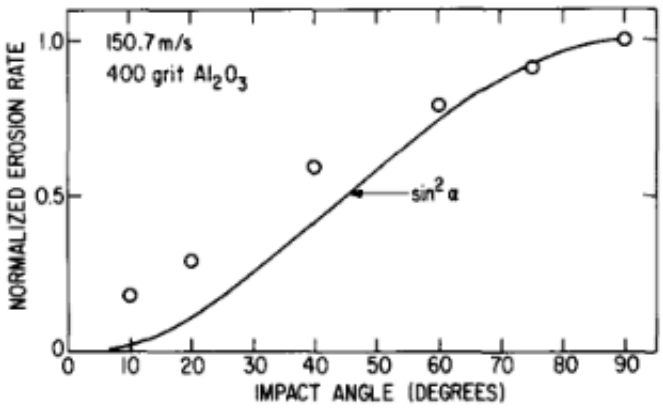

Fig. 2.22 Normalized steady state erosion rate as a function of impact angle in reaction bonded SiC [15].

Fig. 2.22 shows erosion rate of reaction bonded SiC as a function of impact angle that erosion rate increased gradually and reached max. at 90°.The SEM images and the angular dependence of ΔW suggest that plasticity occurs although the damage is predominantly brittle fracture.

2.10.2 Erosion behaviour of SiC/(W, Ti)C laminated ceramic

Jianxin et al.[20] reported that the erosion behaviour of SiC/(W, Ti) laminated ceramic nozzles were better than homologous stress-free ceramic nozzles due to the formation of compressive residual stresses in the entry region of the nozzle. They prepared the nozzles by hot pressing. Due to the difference in thermal coefficient and shrinkage of SiC and (W, Ti) C solid solution, the entry region exhibits compressive stresses. The tensile stress was counteracted by compressive stresses which led to improvement in erosion wear resistance.

2.10.3 Erosion behaviour of SiC and SiC-TiB_2 composites

Kim and Park [19] studied the erosion rates of monolithic SiC ceramics and SiC-TiB_2 prepared by hot pressing with angular SiC particles (50-150μm) at room temperature, velocity (40-100m/s) and impingement angles (30-90°). They observed that in both materials, plastic deformation with grain pull-out occurs on the eroded surface. The erosion rate did not increase with the increase in particle size, presumably due to the erodent fragmentation. Rather, the erosion rate was higher for the SiC-TiB_2 composites with higher fracture toughness but lower hardness compared to monolithic SiC, indicating that the erosion of these materials is largely controlled by the plastic deformation. Large erodent particle size and elevated temperatures are reported to lead to lower erosion rates for SiC-TiB_2 composites when compared against SiC ceramics.

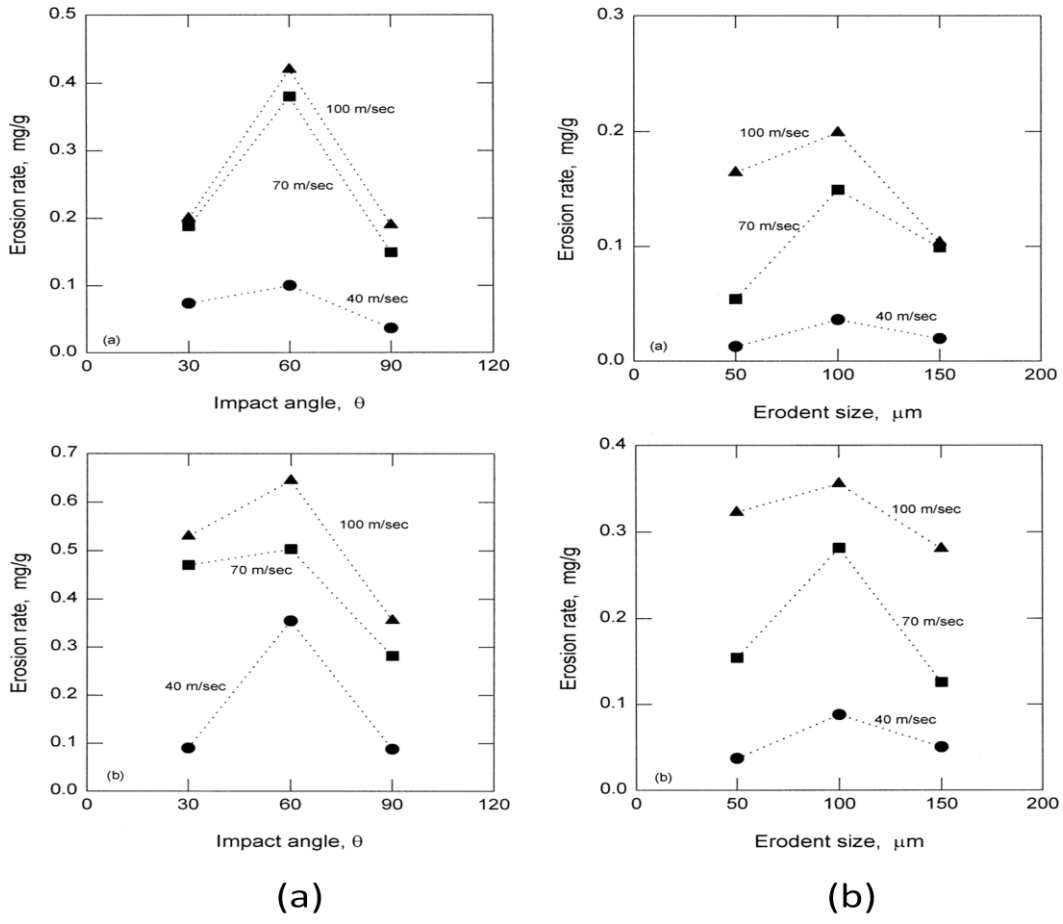

Fig. 2.23 Steady state erosion rate of monolithic SiC containing 5 vol.%Y_2O_3 and SiC composite containing 5 vol.% Y_2O_3 and 14 vol. % TiB_2 as a function of (a) impact angle and (b) erodent particle size at a velocity of 40, 70 and 100 m/s [19].

2.10.4 Erosion of SiC-Si_3N_4 composites

Li et al. [62] studied the erosion behaviour of SiC–Si_3N_4 composites at elevated temperature. The erosion test was performed using SiC particles as erodent with particle size in the range of 325-830μm. They found that the erosion rate of the composites firstly increased and then decreased with increase the erosion temperature. It gradually increased with the increase in impingement angle. The erosion rate was minimum at 1400°C temperature and angle of 30°. The loss of material at low temperature was mainly caused by brittle fracture, while at high temperature the erosion mechanism led to plastic deformation and oxidation protection.

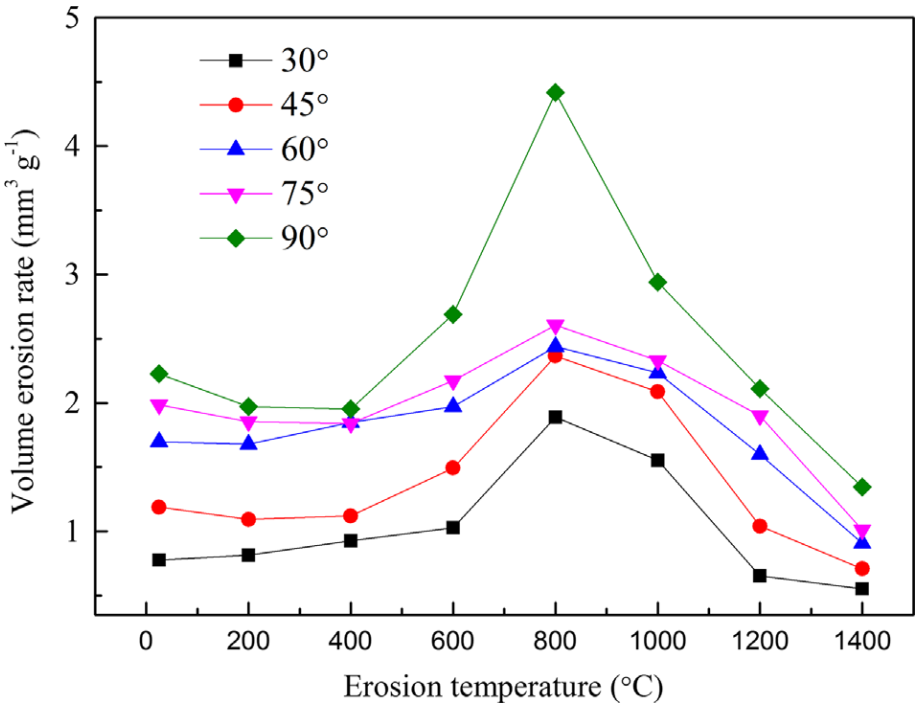

Fig. 2.24 The volume erosion rates of SiC–Si_3N_4 composite ceramic with respect to the erosion temperature and the impingement angle [62].

As shown in **Fig. 2.24**, the erosion rate of SiC–Si_3N_4 composite ceramic largely depends on the angle of impingement. With the increase in angle erosion rate gradually increases and at 90° it is maximum. At lower temperatures, SiC–Si_3N_4 composites erosion occurs by brittle fracture.

2.10.5 Erosion of Si/SiC composites

Amirthana et al. [63] studied the solid particle erosion behaviour on biomorphic Si/SiC ceramic composites. The erodent used were SiC particles (80-450 µm) which is angular in shape and impact velocity and impact angle was varied from 20 to 50 m/s and 20° to 90°, respectively. They found that brittle and cleavage fractures are occured at the erosion surface. The erosion results shows that high erosion occurred at normal angle of impingement while at lower angle less erosion occurred.

2.10.6 Erosion of SiC-WC composites

Sandan et al. [47] reported that the less erosion occurred when SiC-WC composites were eroded at normal incidence by alumina particles compare to silicon carbide particles.

Table 2.5. Erosion rates of SiC–WC composites at normal incidence using alumina and silicon carbide erodent particles [47].

Sample	Erosion rate at normal incidence (mm^3/kg)	
	Alumina	Silicon carbide
SW0	18.31	1044.63
SW30	6.57	850.73
SW50	20.49	1223.24

When eroded by silicon carbide particles, erosion rates of the composites increased with increasing angle of impingement from 30° to 90°, and decreased with the WC reinforcement up to 30 wt%. Eroded surfaces predominantly showed fracture of SiC grains and pull out of WC particles. Distribution of WC particles protected SiC grains from fracture up to 30 wt% WC reinforcement. A minimum erosion wear rate obtained for SiC- 30wt% WC composite.

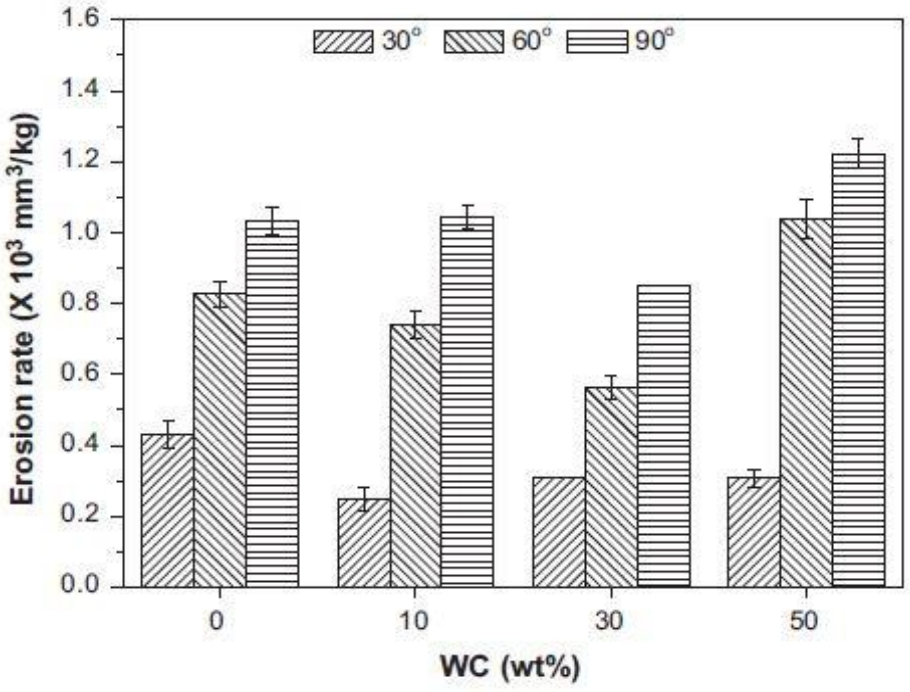

Fig. 2.25 Steady state erosion rates of SiC–WC composites as function of angle of SiC particle impingement and WC content [47].

2.11 Problem formulation

Literature study indicates that the varieties of ceramics can be added to improved mechanical and wear properties of SiC ceramics. The key feature in selecting the reinforcement is that the average properties of SiC matrix should be improved by engineering of microstructure. SiC-TiB_2, SiC-WC/TaC, SiC-Si_3N_4 are studied for their erosion performance. Considering higher modulus and high temperature strength, one would expect an improvement in wear behaviour for TaC reinforced SiC ceramics. However, the effect of TaC addition in erosion wear behaviour of SiC ceramics is not investigated, probably because of the processing difficulties. Such difficulties in sintering of SiC-TaC composites are thought to be overcome by the use of rapid sintering technique, spark plasma sintering and the erosion at high temperatures can be assed. In line of the above, the major objective of the present thesis is to fabricate SiC ceramics with 10, 20 and 30 wt% TaC reinforcement by the spark plasma sintering. The SPS conditions will be optimised to get full density of the composites. The sintered composites will be characterised for their microstructure and mechanical features. The behaviour of the sintered composites will be assessed by eroding SiC particles at ambient and 400°C in air. The wear mechanisms will be studied as function of TaC content and erosion temperature.

CHAPTER 3

PLAN OF WORK

In the present work of research, the SiC ceramics with 10, 20 & 30 wt% TaC addition are prepared using spark plasma sintering technique. Microstructural analysis of all the samples is done using Scanning Electron Microscope (SEM) as well as optical microscope. Also characterization of samples is done using X-Ray diffraction (XRD). The mechanical properties such as hardness and fracture toughness of sintered composites are evaluated. Further, the erosion wear of all the samples is performed at room temperature as well as at elevated temperature.

Hardness measurements are carried out on all the samples before and after the erosion by SiC particles. After erosion, all the eroded samples are analyzed using SEM. The eroded surfaces are studied to find the mechanism of material removal in the selected erosion conditions.

A schematic representation of the plan of work is shown as flow diagram in **Fig. 3.1.**

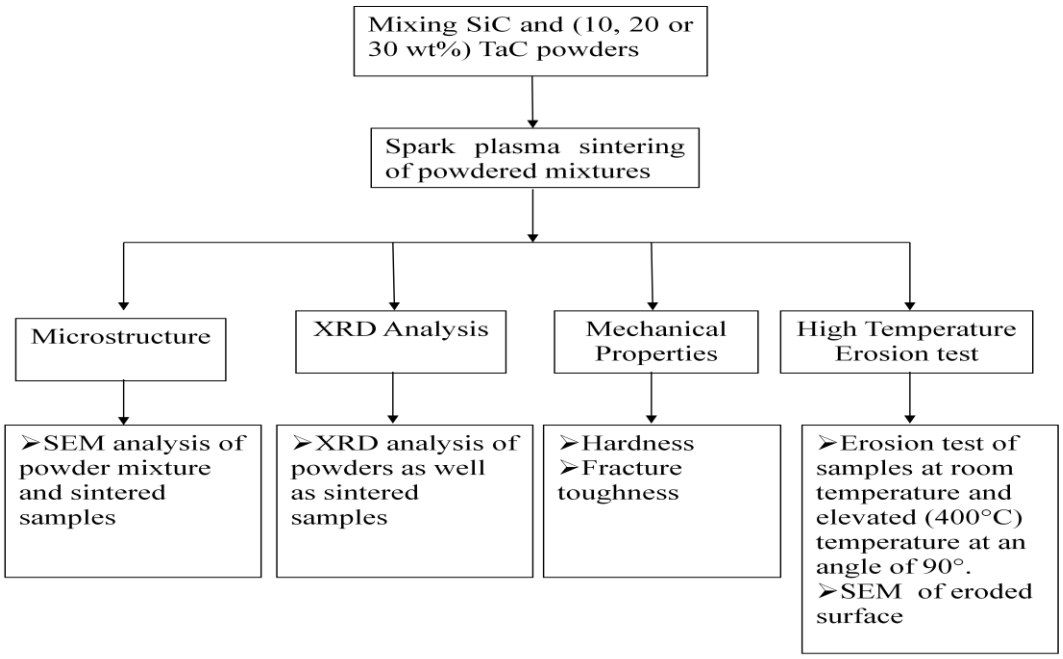

Fig. 3.1 Flow Diagram depicting plan of work

CHAPTER 4

EXPERIMENTAL PROCEDURE

The characterization and high temperature erosion studies of sintered SiC-TaC ceramic composites carried out in the present work are described here:

4.1 Material preparation

Commercially available α-SiC (A1, Showa Denko, Japan) and TaC were used as starting powders. Powder mixture containing 10, 20 or 30 wt% TaC were prepared. The respective powder batches were mixed in toluene for 24 h using WC grinding balls in a polymer jar. The photograph of the tumbler mill is shown in **Fig. 4.1**.The mixed slurry was dried in an oven at a temperature of 100°C for 1 h. After drying, the powder mixture was crushed by mottle & pastel to remove agglomerates. The crushed powder was sieved through a fine sieve to achieve free flow of powders.

Fig. 4.1 Tumbler mill for powder mixing

Simultaneous TG & DSC analysis (TG/DSC Seiko Extar 6300) were carried out on silicon carbide powders as well as tantalum carbide powder and mixture of silicon carbide and tantalum carbide powders in order to identify the occurrence of (any) reaction. All the measurements were carried out in air atmosphere.

The powders were sputter coated with gold, and subjected to microstructural characterization using scanning electron microscopy (SEM S4300, Hitachi Ltd., Japan, or FE- SEM, Quanta 200 FEG, the Netherlands).

Phase analysis of powder mixtures was performed using XRD (XRD, D8 Discover, Bruker AXS GmbH, Germany). A photograph of XRD is shown in **Fig. 4.2**.

Fig. 4.2 X-Ray diffraction machine

The powder mixtures were spark plasma sintered (Dr. Sinter SPS-625, Fuji Electronic Industrial Co. Ltd., Japan) at 1800°C for 5 min at 55 MPa in Ar atmosphere. A photograph of the SPS facility is shown as **Fig. 4.3.**

Fig. 4.3 Spark plasma sintering facility

4.2 Density measurement

The density of the sintered composites was measured by Archimedes principle. For calculating theoretical densities by rule of mixtures, theoretical densities (g/cc) of as received powders considered as per the following formula

$$\frac{1}{D} = \frac{x_1}{d_1} + \frac{x_2}{d_2} \quad \text{..... (4.1)}$$

D= Density of ceramic composite

x_1, x_2 = Weight fraction of respective powders.

d_1, d_2 = Density of respective powders.

Details of batch composition and theoretical density of powder mixture is given in **Table 4.1.**

Table 4.1. Batch composition and density of samples

Sample designation	α- SiC (wt %)	TaC (wt %)	Theoretical density (g/cc)
ST10	90	10	3.5
ST20	80	20	3.8
ST30	70	30	4.2

After the sintering, the samples were removed by hydraulic press and graphite layer was removed from the surface of the sample by using belt polishing. After removing the graphite layer sintered sample was polished on auto polisher by using diamond suspension. Firstly sample was polished on 45µm plate for 25-30 min. After that the sample was polished on 15µm, 6µm plate and finally up to 1µm plate. Photographs of belt polishing machine and auto polisher are shown in **Fig. 4.4**.

(a) **(b)**

Fig. 4.4 (a) Belt polishing machine (b) auto polisher

The phase analysis of the sintered composites was done by using X-ray diffractometer. The microstructural characterization of the polished was done using SEM-EDX analysis.

4.3 Hardness analysis

The micro-hardness of polished samples was measured by Vickers indentation (Leica, VMHT (MOT), Germany) at a 20 N load for a dwell time of 15s for sintered as well as eroded samples. All the readings of hardness were taken at different locations at same load of 20 N. Normally, the average of 10 readings of hardness is reported. A photograph of the instrument which is used to measure the hardness is shown in **Fig. 4.5**.

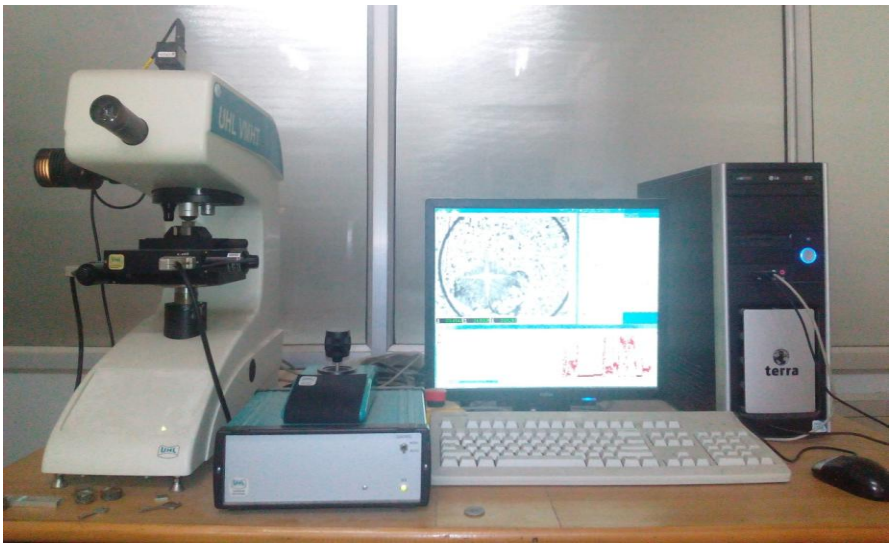

Fig. 4.5 Vickers micro-hardness tester

4.4 Fracture toughness

When indenter indents the samples in hardness test, then some crack is generated. Lengths of crack generated by Vickers indentation (AVK-C2, Akashi Corporation, Japan) at a 20 N load for 15s were measured and fracture toughness (K_{IC}) in $MPam^{½}$ was calculated by using Anstis equation [64]:

$$K_{Ic} = 0.016 * \left(\frac{E}{H}\right)^{1/2} * \frac{P}{c^{3/2}} \quad \text{..... (4.2)}$$

Where c = (L/2)+a. L is length of the diagonal of the indentation, P is load in N, c is crack length in m and H is hardness in GPa. E is elastic modulus of composite in GPa estimated by rule of mixture using elastic modulii of 410 GPa for SiC and 480 GPa for TaC. A schematic representation of cracks generated by Vickers indentation is shown in **Fig. 4.6**.

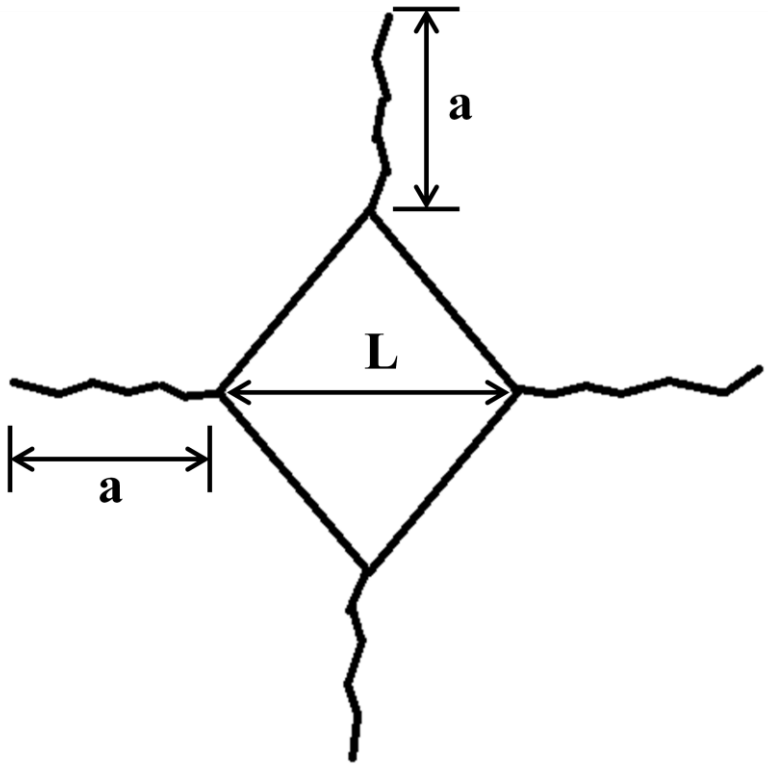

Fig. 4.6 Crack generated by Vickers indentation

4.5 High temperature erosion tester

Erosion tests were performed using a high temperature erosion testing machine. Silicon carbide erodent particles 45-75 µm in size were dried in an oven at 100 °C for 1 h and were mixed with air. The mixed air jet passed through nozzle of 1.5 mm diameter and was subjected to erode the polished surface of the composite at a stand-off distance of 10 mm.

Air pressure was controlled to maintain the particle velocity at 50 m/s with a flow rate of 3 g/min. Erosion tests was performed at impingement angles of 90° at room temperature and elevated temperature (400°C). A schematic diagram of high temperature erosion set up is given in **Fig. 4.7** and the erosion test parameters are listed in **Table 4.2**.

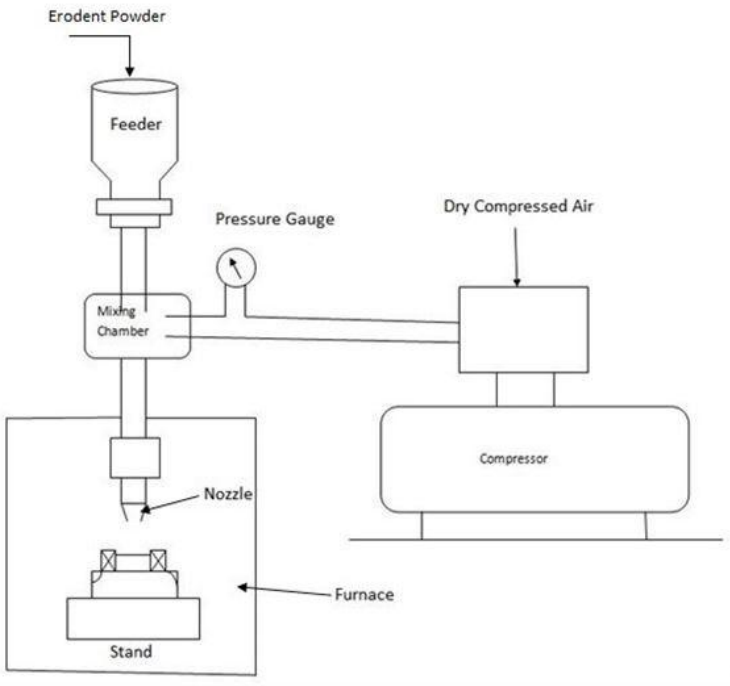

Fig. 4.7 Schematic diagram of high temperature erosion tester

The weight loss of the sintered ceramics was measured to an accuracy of ±0.1 mg. The average weight loss was converted to average volume loss and erosion rate E in mm^3/kg was determined using the following formula:

$$E = \frac{V}{M} \quad \text{..... (4.3)}$$

where V is volume of the material removed in steady state in mm^3 and M is the mass of erodent particles used in steady state in kg. The erosion results were checked for the reproducibility by conducting whole experiment at least twice for each composition. Material removal mechanisms were elucidated using SEM-EDS analysis of eroded surfaces.

Table 4.2. Experimental parameters for high temperature erosion test

Erodent material	Impact velocity	Temperature	Impact angle	Discharge rate	Test duration
Silicon carbide particles (45-75µm)	50 m/s	• Room temperature • 400°C	90°	3 g/min	15min

CHAPTER 5

RESULTS & DISCUSSION

5.1 TGA and DSC analysis

Fig. 5.1 shows the TGA and DSC curves for SiC and TaC powder as well as mixture of SiC and TaC powders in a temperature range of 30°C to 1430°C.The diagram shows that SiC powder did not change weight up to the temperature of around 1150°C. After reaching to this temperature, the weight slowly increased. For TaC powder the weight is same up to 588°C. After that weight rises from 588°C to 755°C. After reaching at 755°C, there is no increase or decrease in weight of tantalum carbide. The TGA curve of powder mixture shows that weight remains same up to 610°C. After that, weight increased in from 610°C to 751°C. After reaching 751°C, weight remains constant up to 1180°C. After that again weight gains up to 1430°C.

DSC curve of silicon carbide, tantalum carbide powder and mixture of silicon carbide and tantalum carbide powder shows an endothermic peak in each case. The endothermic peak exists for pure tantalum carbide at a temperature of 769°C. The peak is observed in the temperature range of 700°C to 770°C for powder mixture.

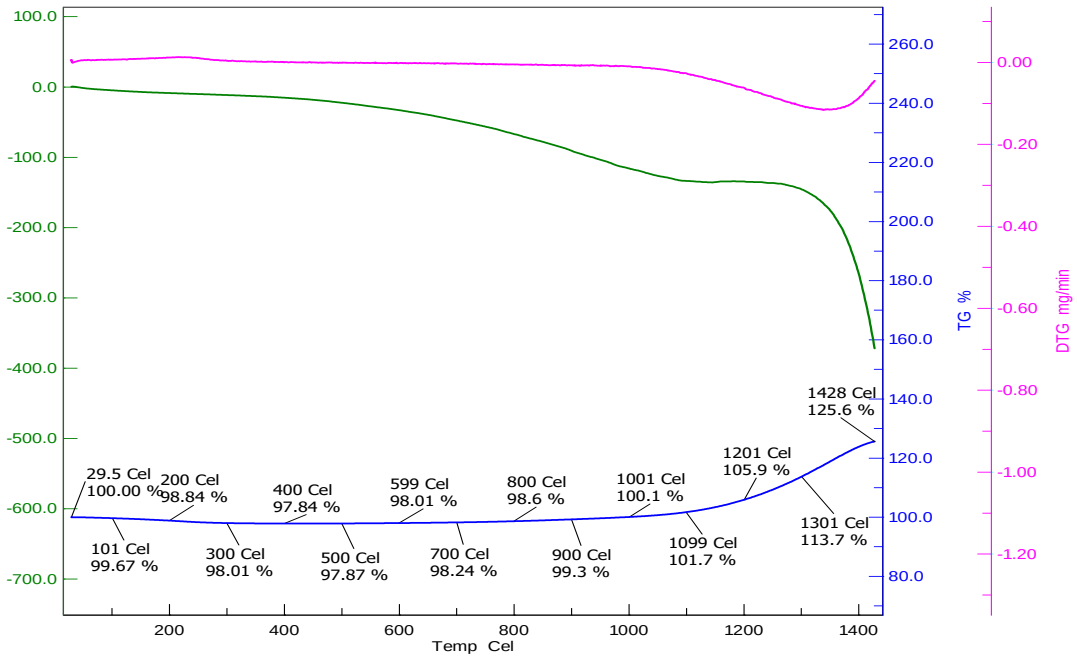

(a)

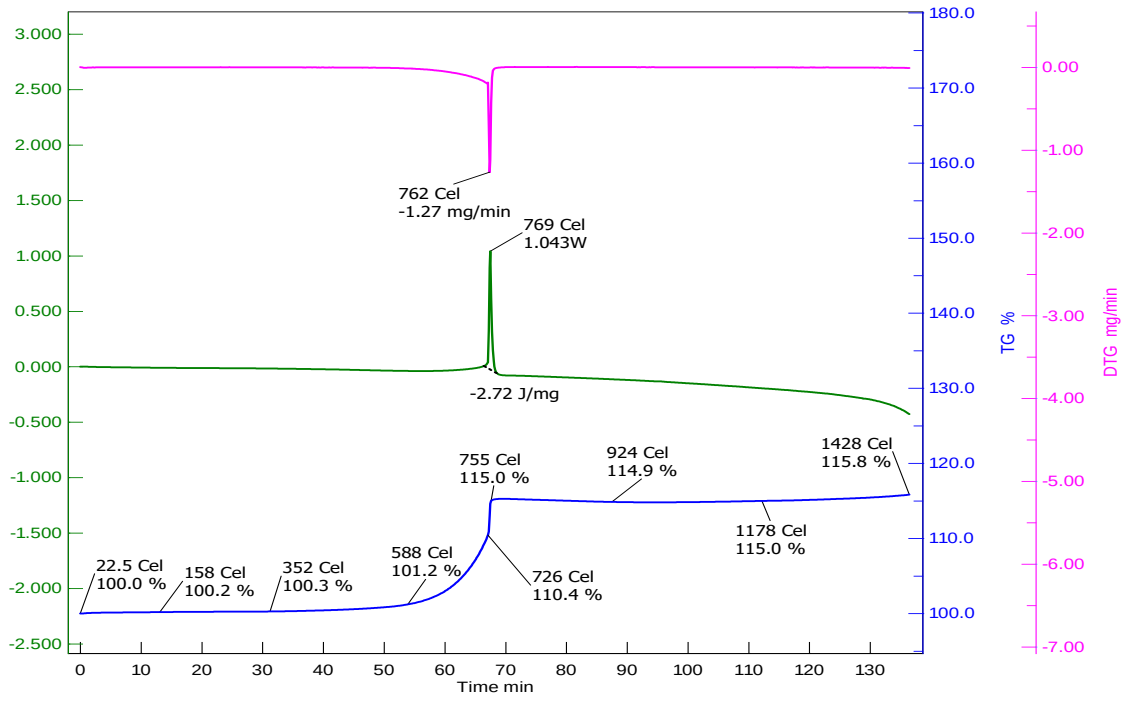

(b)

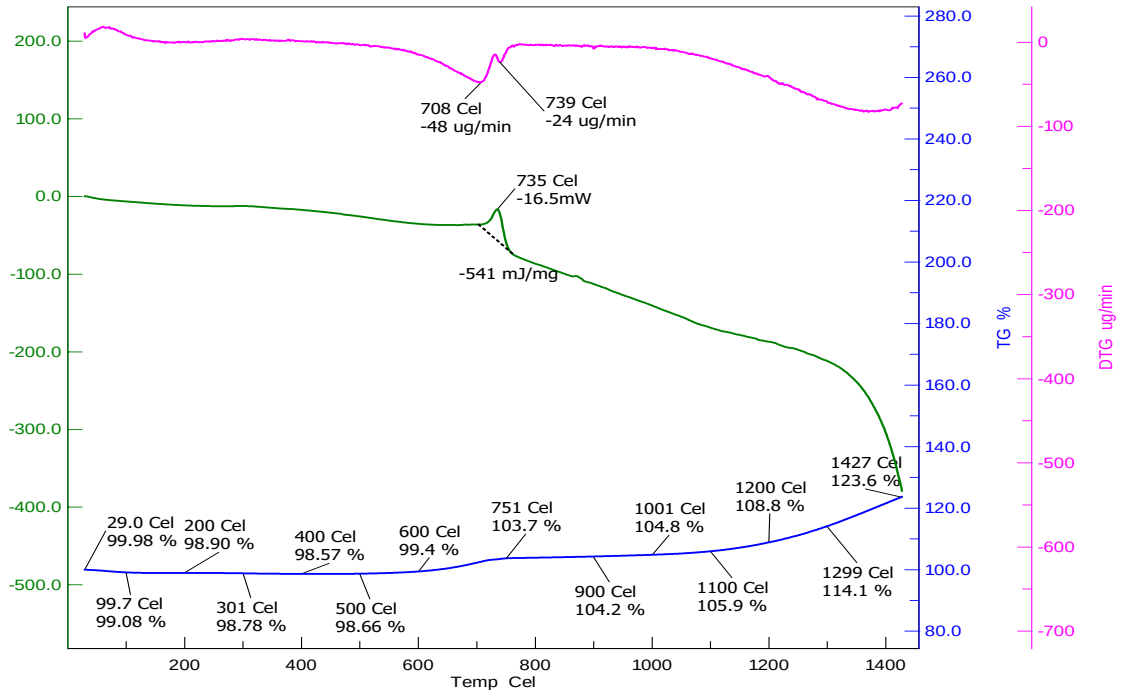

(c)

Fig. 5.1 TGA & DSC curves for (a) SiC powder (b) TaC powder (c) powder Mixture of SiC and TaC

5.2 Microstructural characterization of powders

Fig. 5.2 shows the microstructure of as received powder of SiC and TaC as well as the mixture of SiC and TaC powders. Microstructure shows that there is uniform distribution of TaC particles in SiC matrix. The particle size of SiC particles is in the range of 400-600nm while for TaC particles is 0.3-1.5µm. The concentration of TaC particles in the composites increased with increasing TaC content in the initial powder mixture. The microstructures show that the particles are nearly equi-axed in shape and no elongated grains are present.

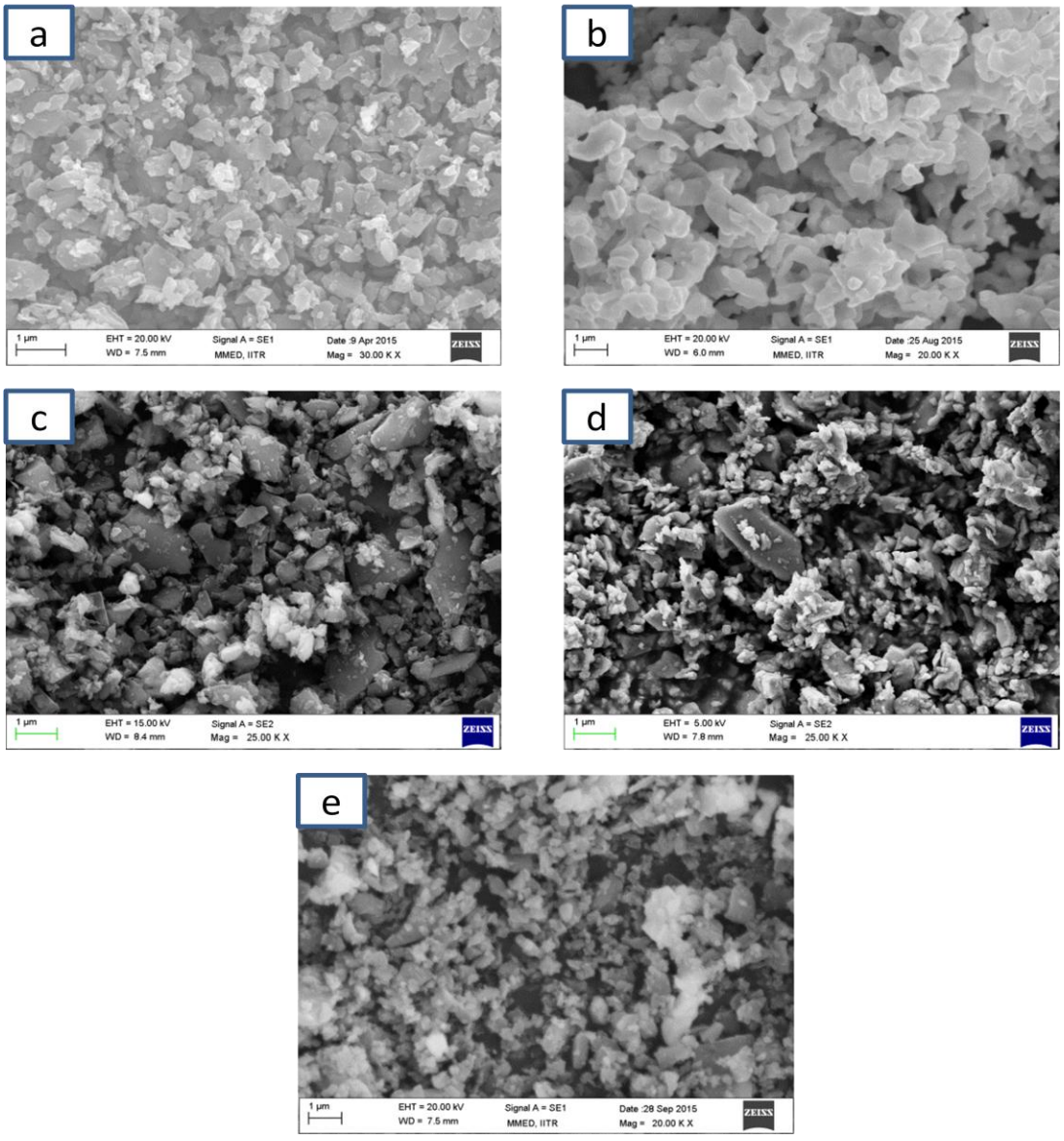

Fig. 5.2 SEM images (a) SiC powder (b) TaC powder (c) powder mixture of SiC-10wt% TaC (d) powder mixture of SiC-20wt% TaC (e) powder mixture of SiC-30wt% TaC

EDX analysis of powder mixture as well as sintered composites is shown in fig. EDX analysis of mixing powder shows that there is no oxygen present. The mapping of elements shows the distribution of each elements and only Si, Ta and C elements are present.

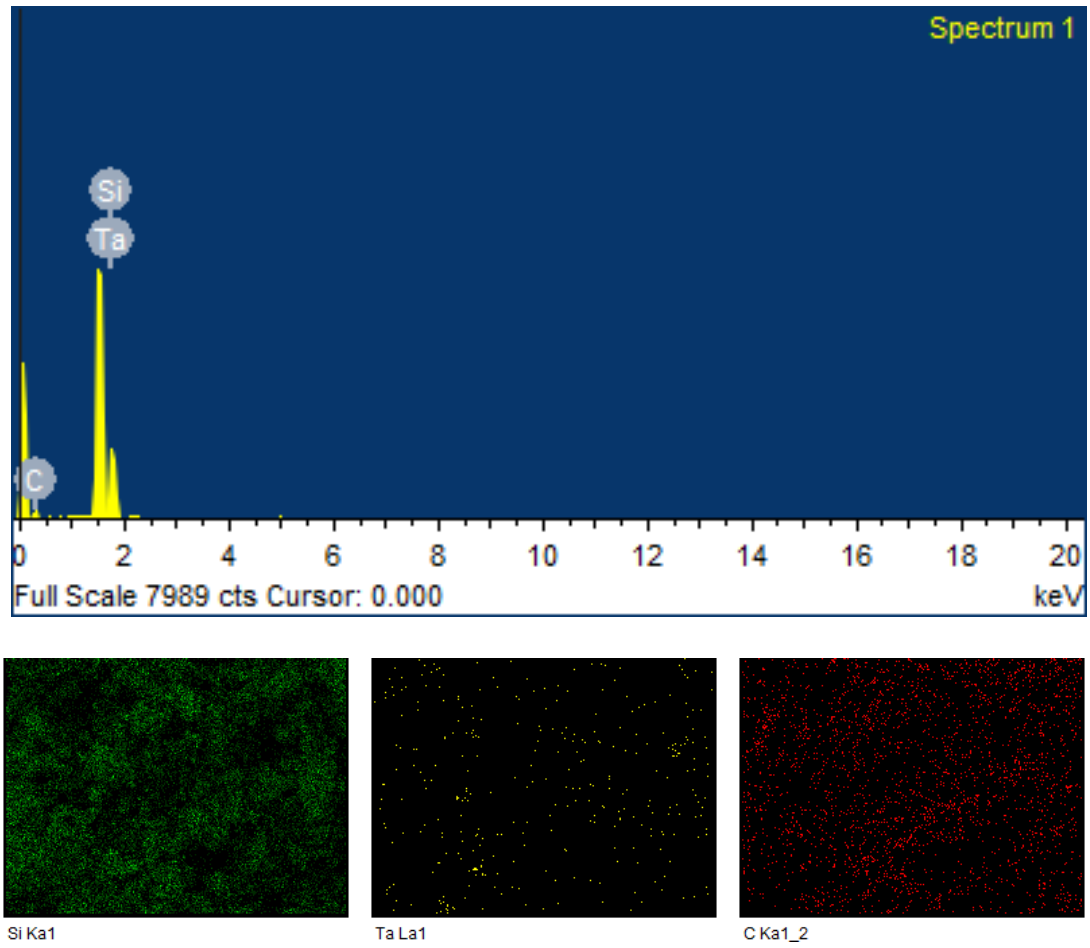

Fig. 5.3 EDX analysis of powder mixture and mapping of elements

5.3 XRD analysis of powders

The XRD patterns of powder mixture of SiC and TaC are shown through **Figs.5.4-5.6**. The XRD pattern of monolithic SiC and TaC are also given. XRD reveals that only hexagonal SiC and cubic TaC phases are present in composites. The peak intensity of TaC is identical with the intensity of starting powder in different composites shows that chemical composition is identical. XRD shows the good chemical compatibility between 6H–SiC and TaC. Therefore, two-phase SiC-TaC compositions are produced by spark plasma sintering of SiC and TaC powder mixtures.

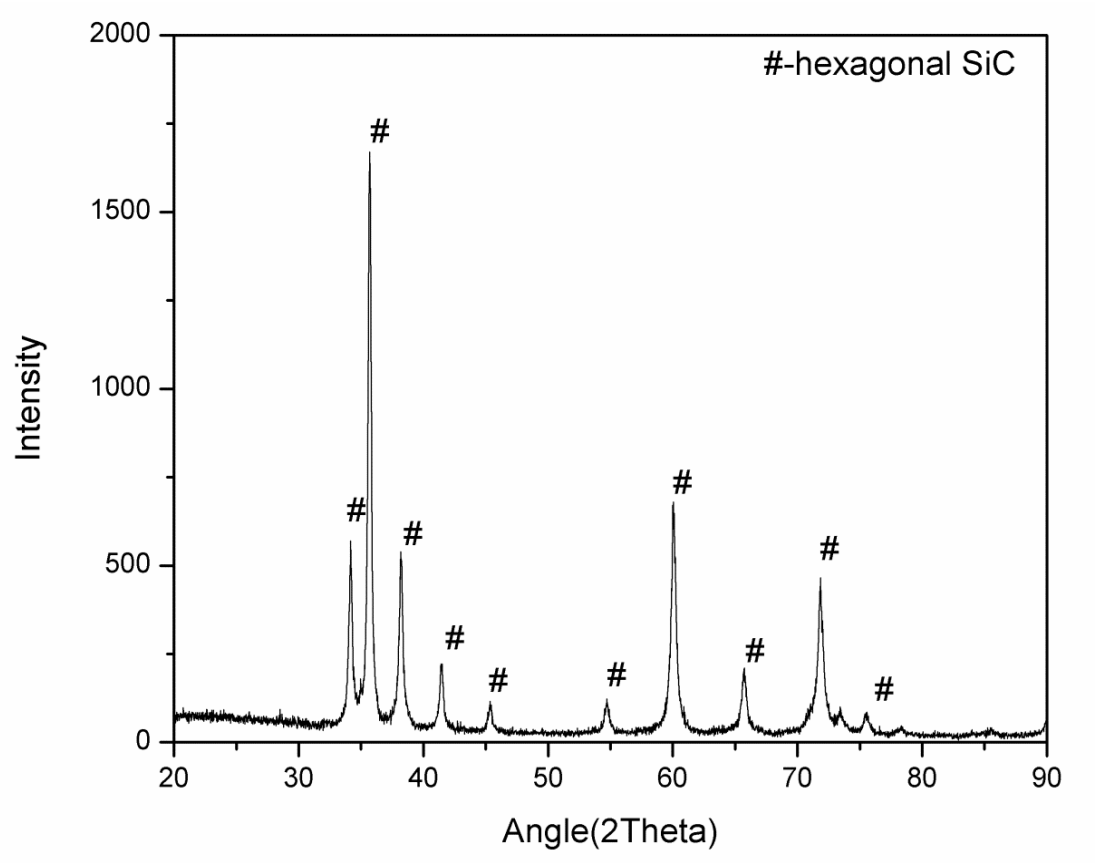

Fig. 5.4 XRD patterns of SiC powder

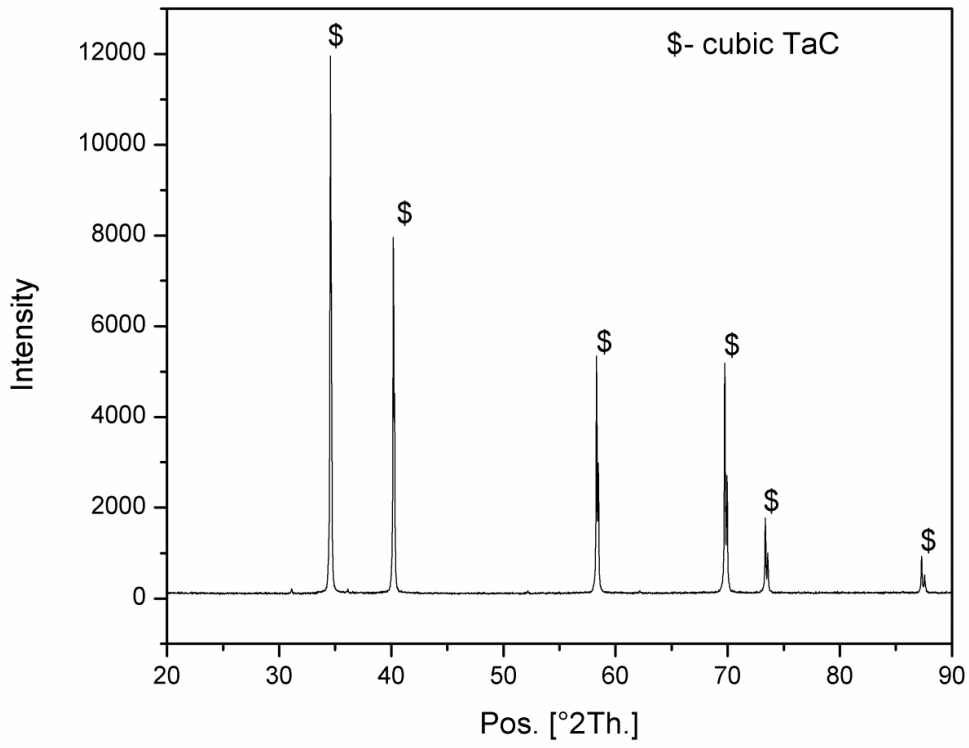

Fig. 5.5 XRD patterns of TaC powder

XRD patterns of powder prepared of SiC with 10, 20 &30 wt% TaC are shown in **Fig. 5.6.** XRD analysis reveals no other phase than SiC & TaC. It is possible that the peak intensity of any other minor phases is out of the detection limit of the XRD instrument. Furthermore, the intensity of SiC & TaC peaks is increased. XRD shows that the peaks of TaC is increased while SiC peaks decreased with the increase TaC content from 10 to 30 wt%.

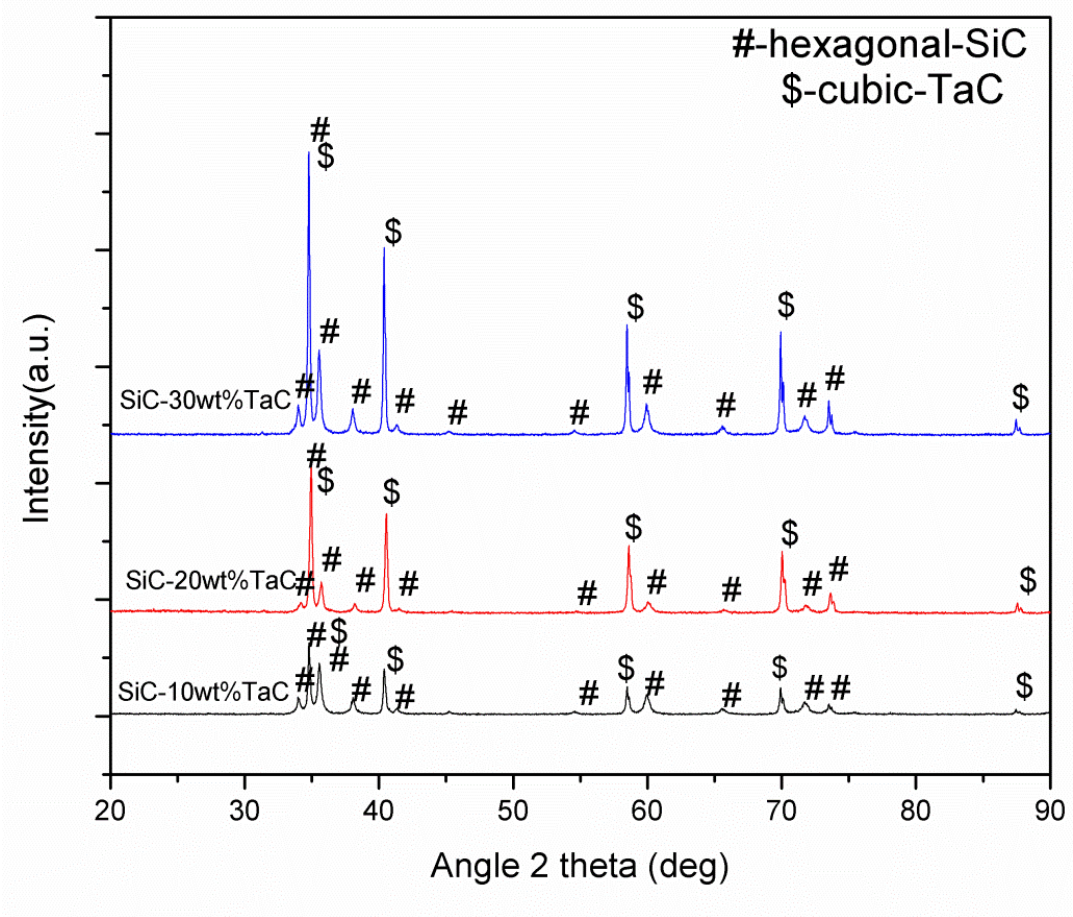

Fig. 5.6 XRD patterns of powder mixtures of SiC and TaC

5.4 Sintering behaviour

The powder mixtures are sintered by SPS at a temperature of 1800°C at a pressure of 55 MPa and holding time for 5 minutes. **Fig. 5.7** shows the sintering behaviour of the samples. The curve shows densification with respect to temperature. In first stage, temperature rises from 575°C to 600°C in 6 minutes. After that in second stage temperature rises from 600°C to 1800°C in next 12 minutes with a heating rate of 100°C/min and pressure rises up to 55 MPa.

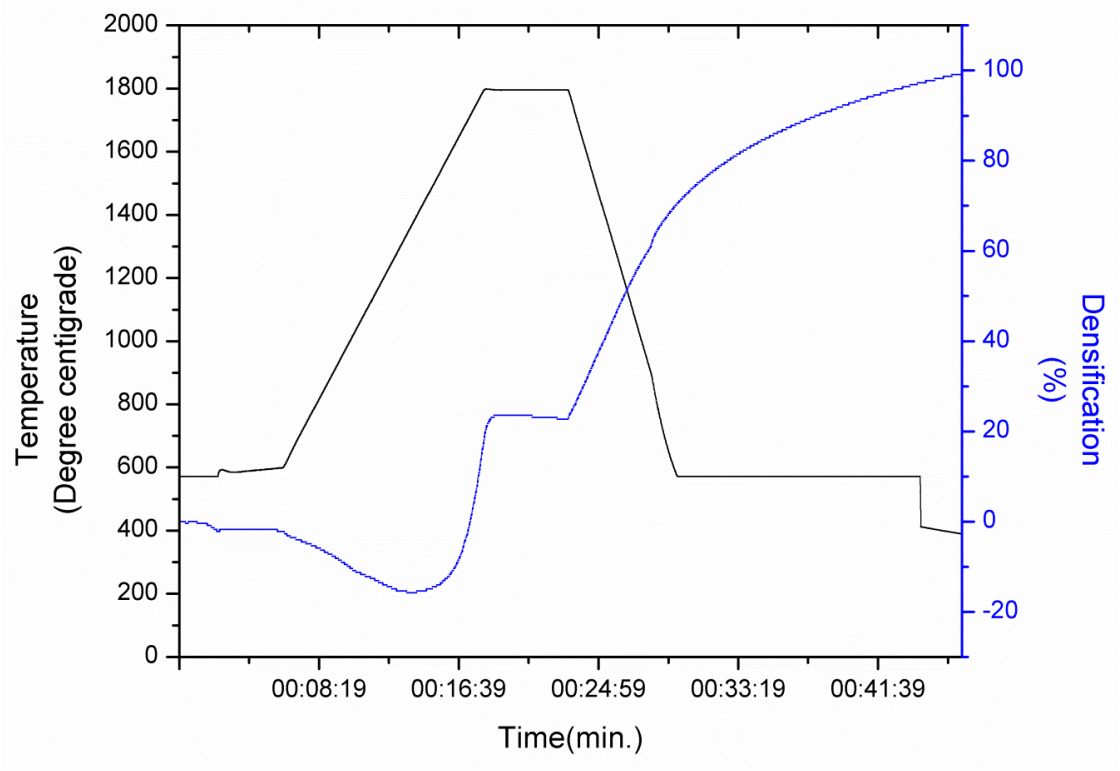

Fig. 5.7 Sintering behaviour of SiC-TaC composites

After that, sample is held at 1800°C temperature for next 5 min to densification. After holding 5min at 1800°C, temperature is reduced with a cooling rate of 200°C/min up to 900°C. After that normal cooling takes place and densification of material is continuous. The densification curve shows that densification starts at around 1500°C increases up to 1800°C. There is no further densification during holding. When holding time is over further densification takes place. It is clear that the densification takes place up to 100%.

5.5 Microstructural characterization of sintered composites

Typical microstructures of the sintered samples are shown in **Fig. 5.8**. Microstructures of sintered samples show that TaC particles are homogenously distributed in SiC matrix. The size of TaC particles is in the range of 0.4-2.2µm. With the increase in the concentration of TaC, the average distance between TaC particles is decreased from around 8µm to 4µm. The particles are nearly equi-axed in shape in sintered composites.

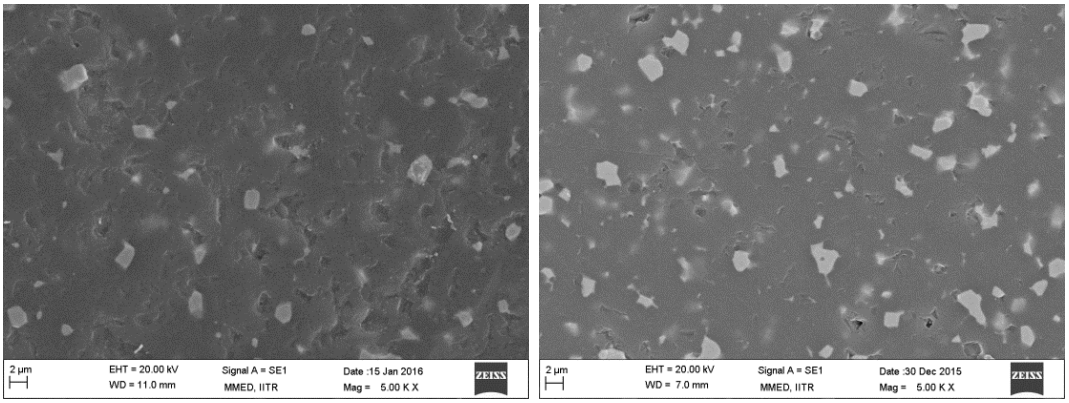

(a) **(b)**

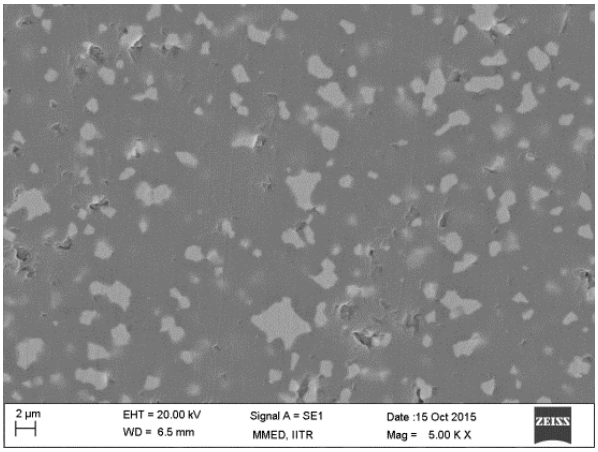

(c)

Fig. 5.8 SEM images of the sintered SiC-TaC composites (a) 10wt%TaC (b) 20wt% TaC (c) 30wt% TaC

EDS analysis of sintered sample shows that there is no oxygen present. There is a uniform distribution of TaC particles in SiC matrix. Si, C, & Ta elements are present. The mapping of elements show that how the distribution of elements in the sample.

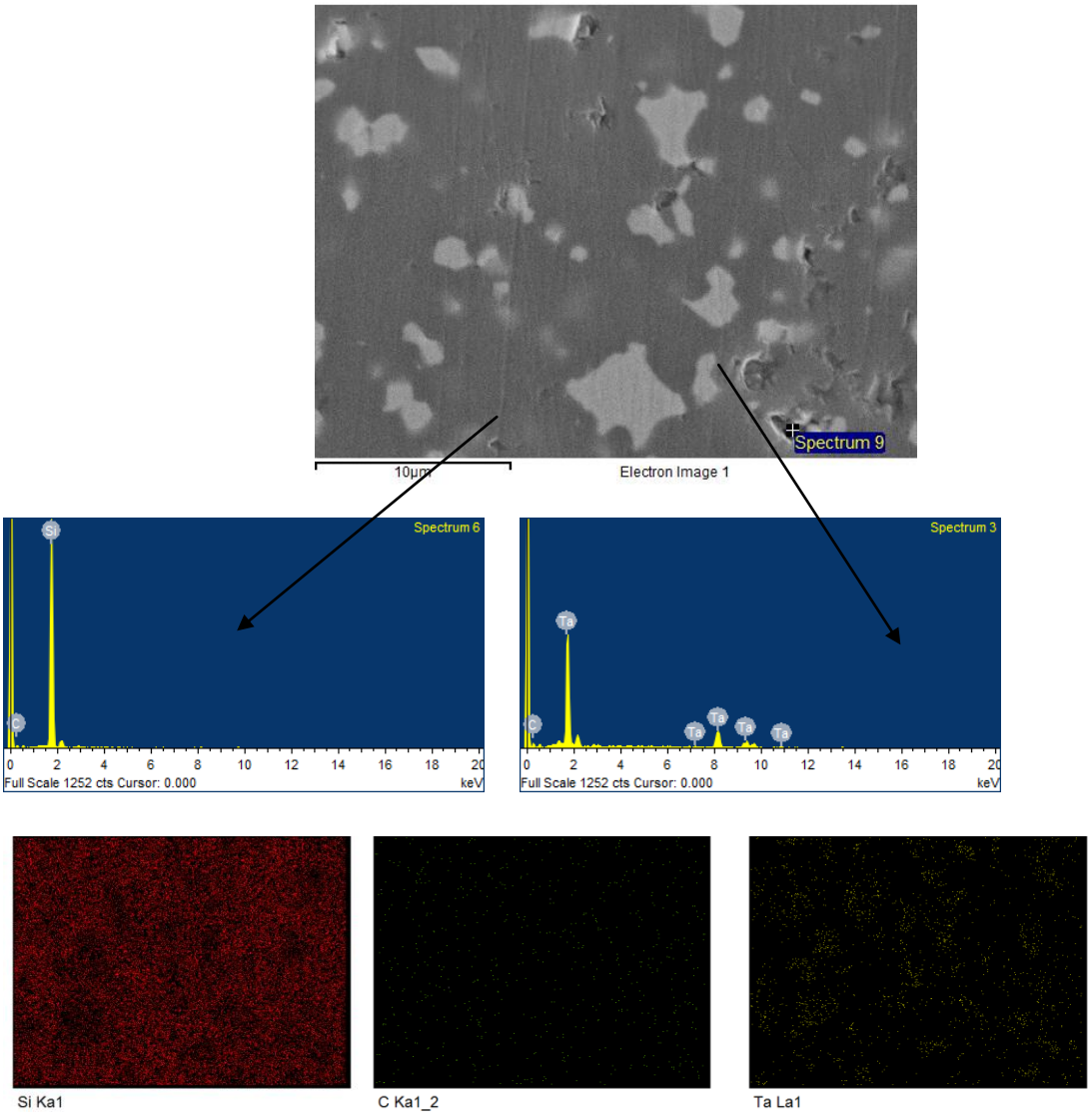

Fig. 5.9 EDX analysis of sintered composites and distribution of elements

5.6 XRD analysis of sintered composites

The XRD patterns of sintered SiC-TaC composites are shown in **Fig. 5.10**. XRD reveals that only hexagonal SiC and cubic TaC phases are present in composites. The peak intensity of TaC is identical with the intensity of starting powder in different composites shows that chemical composition is identical.

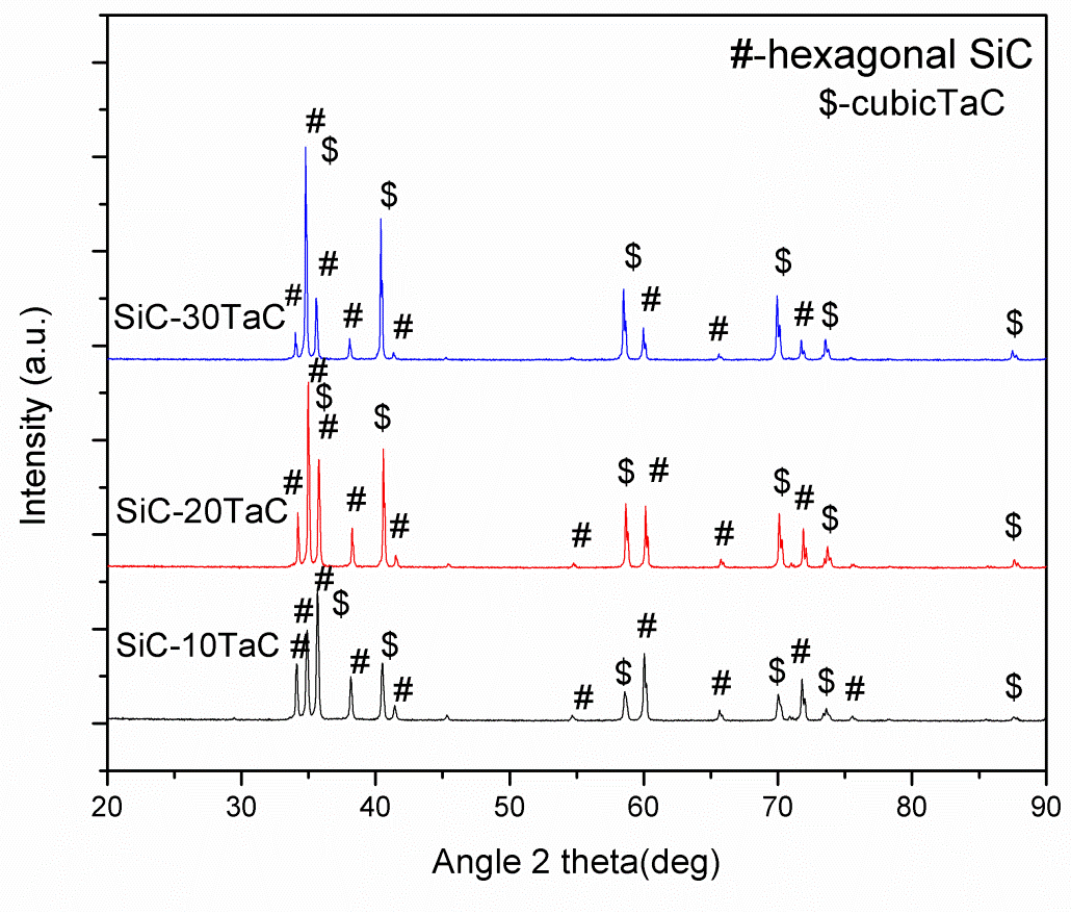

Fig. 5.10 XRD patterns of sintered SiC-TaC composites

It is possible that the peak intensity of any other minor phases is out of the detection limit of the XRD instrument. Furthermore, the intensity of TaC peaks is increased while that of SiC peaks decreased with increase in TaC content from 10 to 30 wt%.

5.7 Mechanical properties

The estimated hardness and fracture toughness values of the investigated composites are listed in **Table 5.1**. The value of hardness is decreased with increase in TaC. The highest value of hardness is 25.75 GPa for ST10, 24.60 GPa for ST20 and 23.30 GPa for ST30. Fracture toughness is increased with the increase in TaC content.

Table 5.1 Mechanical properties of SiC-TaC composites

Sample designation	Hardness (GPa)	Fracture toughness ($MPam^{1/2}$)
ST10	25.75±0.55	3.48±0.30
ST20	24.60±0.63	3.52±0.26
ST30	23.30±0.55	3.85±0.23

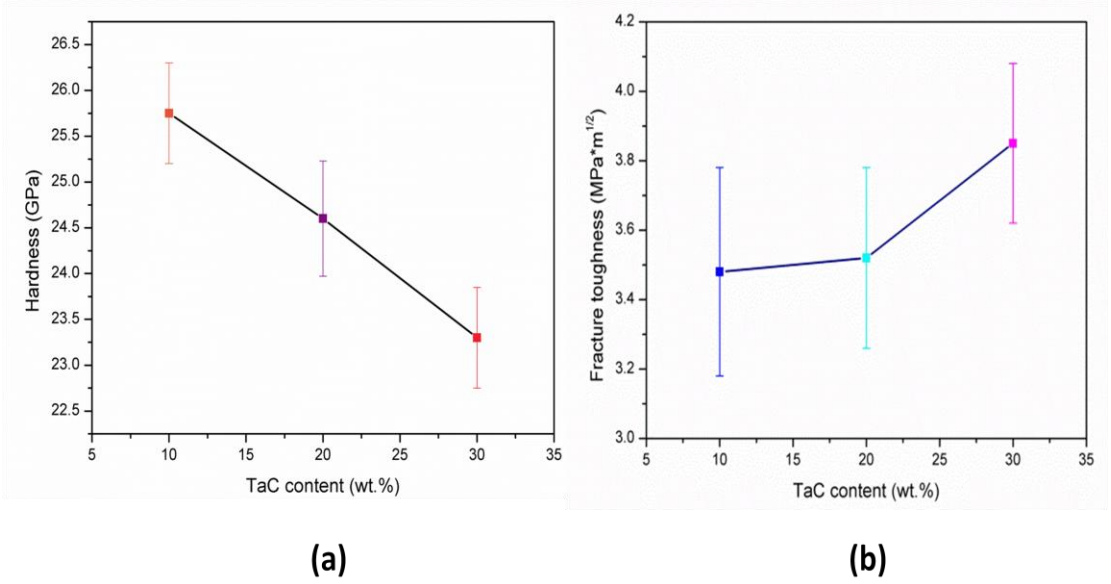

Fig. 5.11 Variation of (a) hardness and (b) fracture toughness with TaC content in SiC-TaC composites

5.8 Crack propagation in samples

Crack propagation in after Vickers indentations for the SiC-TaC composites are shown in **Fig. 5.12**. The TaC phase appears bright, while the SiC phase looks gray. The identity of the major elements in each of these constituents was confirmed by EDX analysis. Crack deflection as well as crack bridging by TaC is appeared which leads to the toughening of SiC ceramic composites.

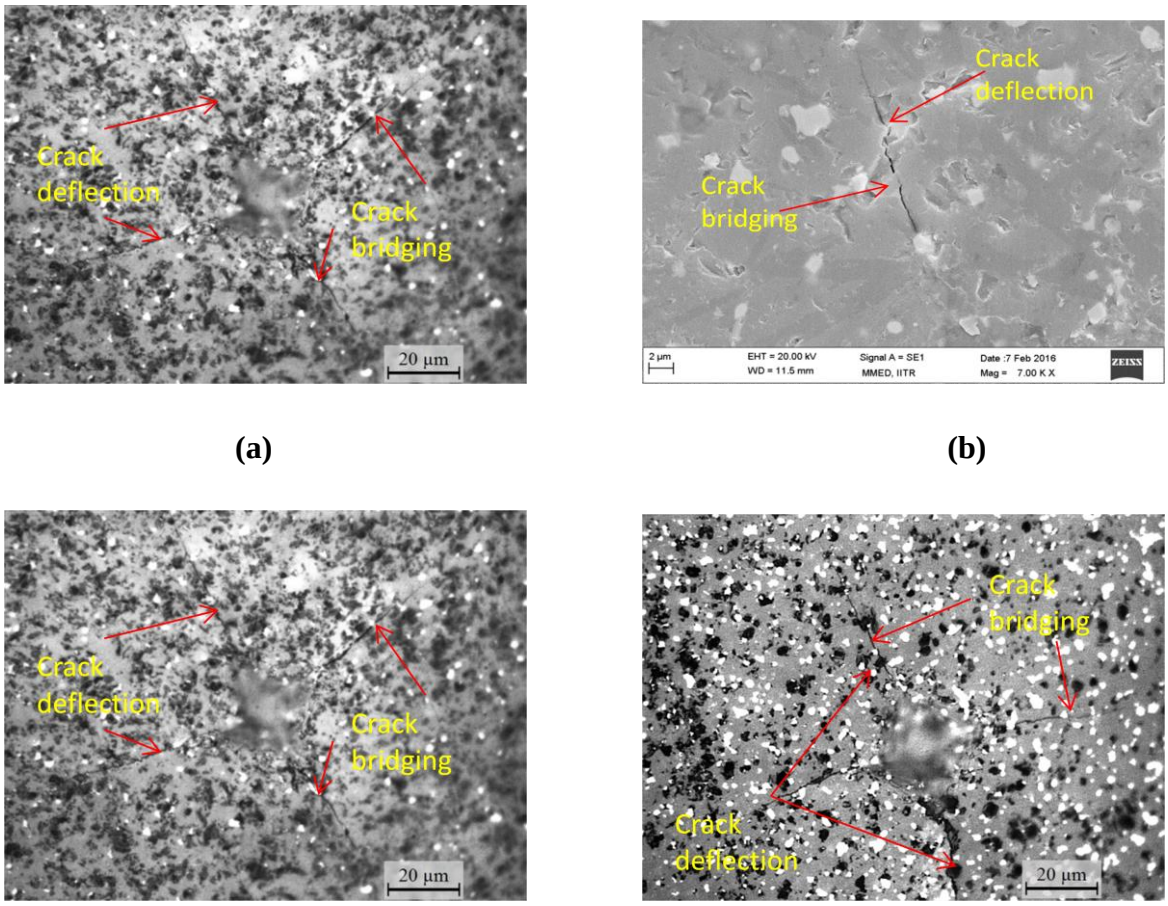

Fig. 5.12 Crack propagation in Samples (a) & (b) ST10 (c) ST20 (d) ST30

5.9 Erosion of SiC-TaC composites

Erosion test is performed on the sintered composites for 15 minutes using silicon carbide as the erodent. The weight loss of the composites measured and erosion rate is calculated. Erosion rate of the SiC-TaC composites at 90° angle of impingement varied from 53 to166 mm^3/kg. The maximum erosion rate observed for the ST10 composite while erosion rate is the minimum for ST30. The erosion rate of all three compositions is given in **Table. 5.2** and **Fig. 5.13.**

Table 5.2 Erosion rate of the sintered SiC-TaC composites

Sample	Erosion Rate (mm^3/kg)	
	Ambient Condition	400°C
ST10	96	166
ST20	71	120
ST30	53	94

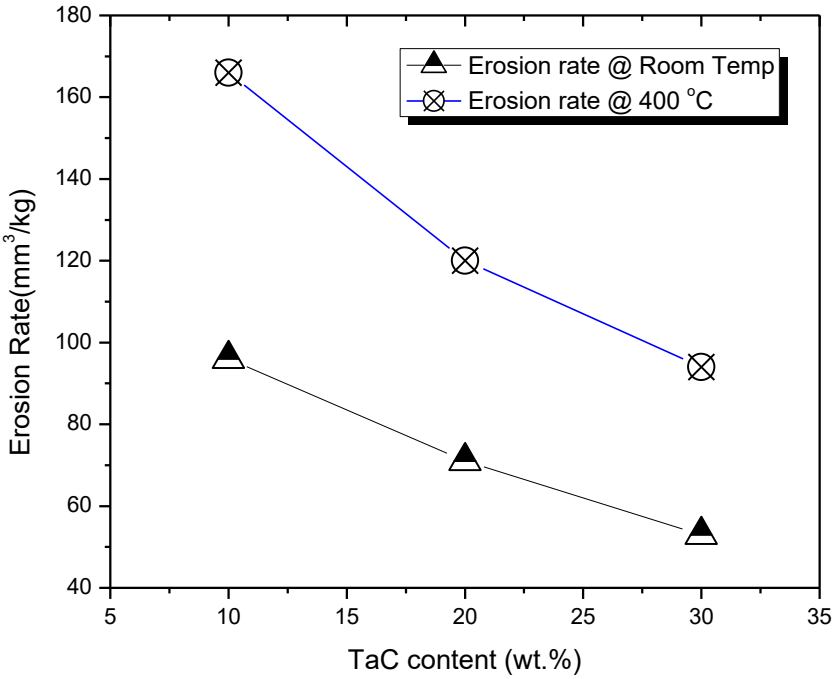

Fig. 5.13 Erosion rate of SiC-TaC composites with TaC content and temperature

5.10 Eroded surface analysis

Eroded surface of the samples shows pull-out of TaC particles and brittle fracture of SiC matrix at room temperature as well as 400°C. The fracture is dominant at 90° angle and shows mixed mode of fracture intergranular and transgranular. The eroded surface of samples shows intergranular and transgranular fracture. Eroded surface shows that higher fracture occurs in ST10 composites at 400°C temperature.

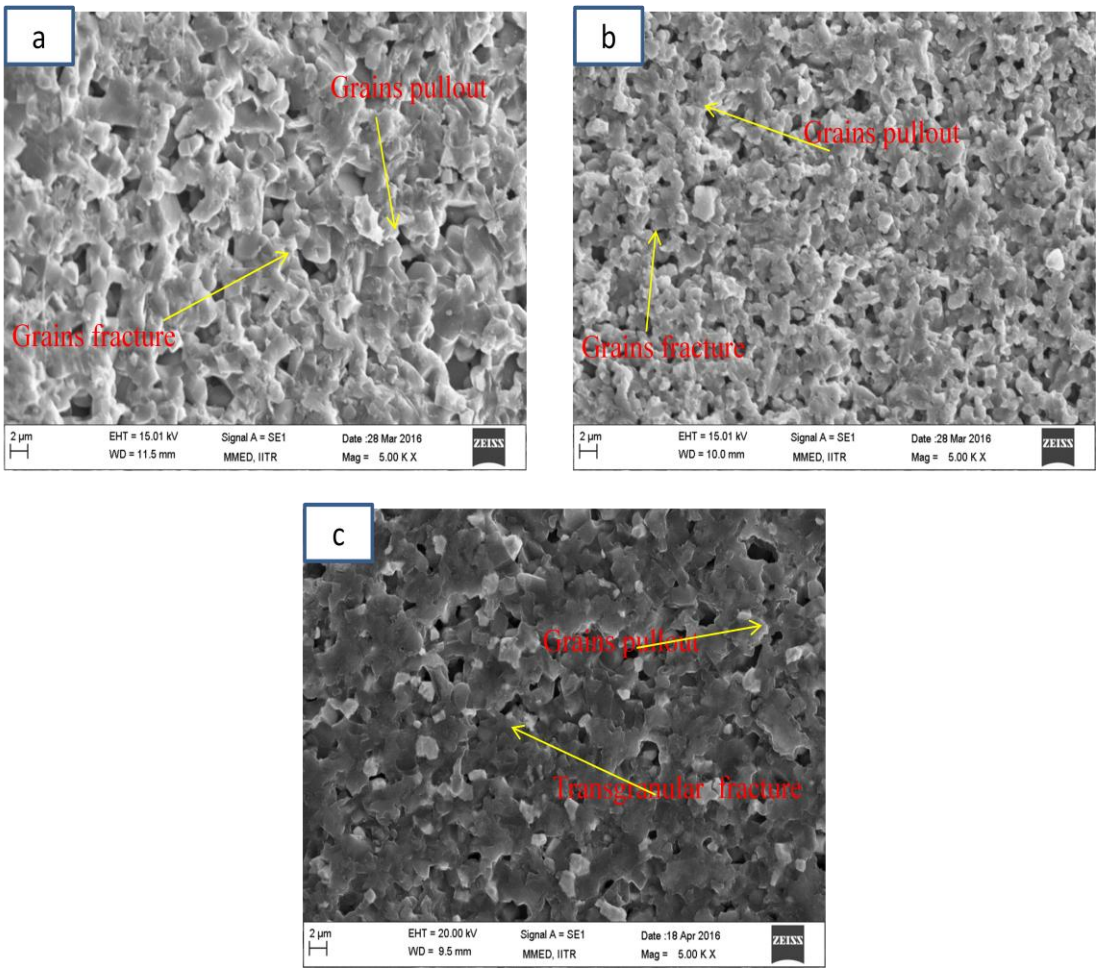

Fig. 5.14 SEM images of surface of samples eroded at room temperature (a) ST10 (b) ST20 (c) ST30

Surfaces of composites eroded at room temperature and 400^{o}C are shown in **Figs. 5.14 and 5.15**, respectively. It is clear from **Fig. 5.14** that highest fracture occurs in SiC with 10 wt% TaC composites and minimum for the SiC with 30 wt% TaC addition. **Fig. 5.15** shows the eroded surface of the composites at 400°C temperature. It is clear that at higher temperature erosion also increases and more fracture occurs as compared to ambient condition. The reason for the higher erosion at 400°C as compared to ambient, as temperature increases matrix of material becomes soft or hardness of the material reduced. Due to the hardness reduced more fracture occurs and more SiC grains pull-out in ST10 as compared to ST30. In ST30 TaC particles hold the grain boundary and provide strength for composites not to pull-out of SiC grains.

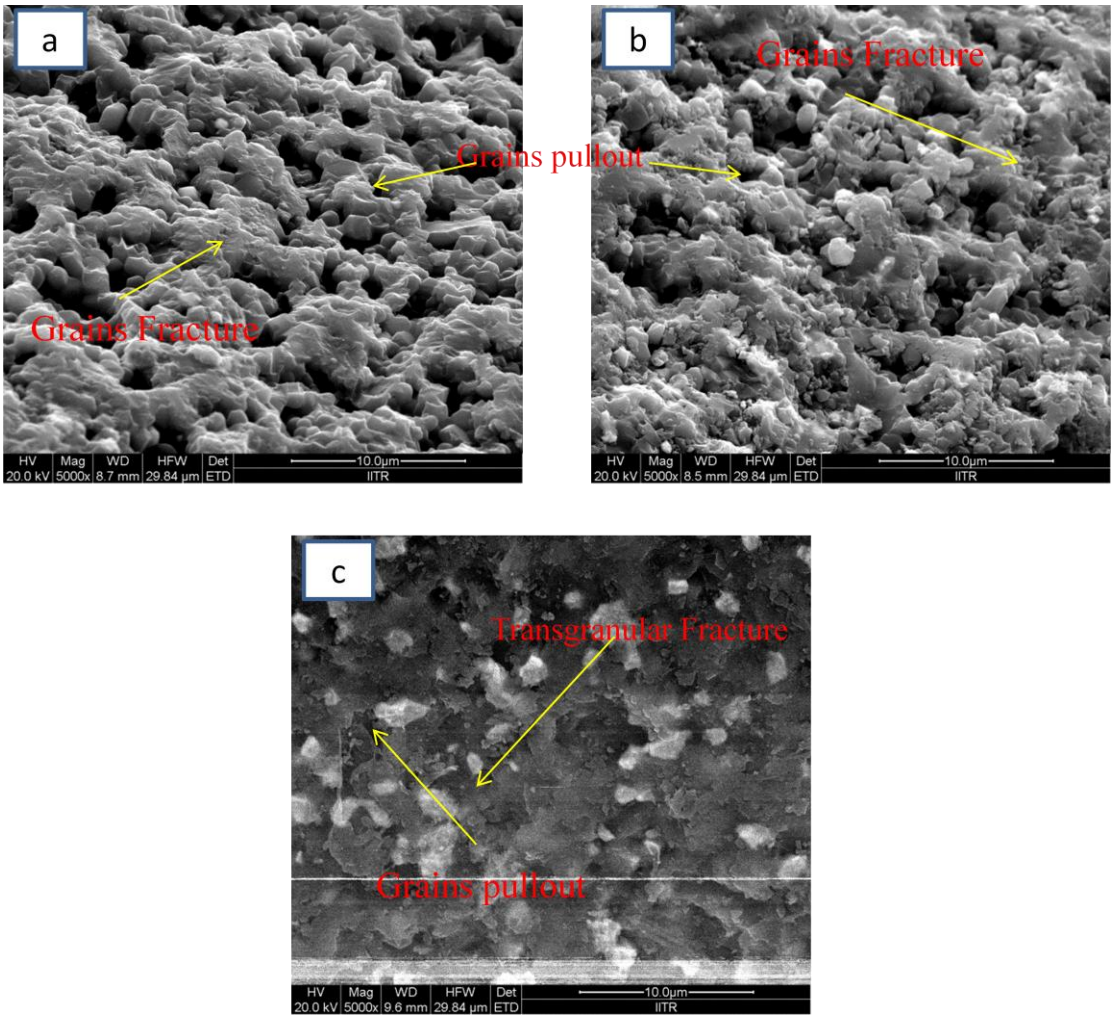

Fig. 5.15 SEM image of surface of samples eroded at 400°C temperature (a) ST10 (b) ST20 (c) ST30

CHAPTER 6

CONCLUSIONS

Powders of α-SiC and TaC were sintered by spark plasma sintering at 1800°C temperature at a pressure of 55 MPa in Ar atmosphere holding time for 5 minutes to obtain highly dense SiC-TaC composites. Sintered composites were tested in erosion by SiC particles (45-75 μm size) in ambient and elevated temperature (400^{o}C) in air. The following conclusions are obtained from the characterization and erosion wear of the composites.

(a) The relative density of the composites obtained was more than 99%.

(b) The fracture toughness increased with the addition of TaC content and maximum fracture toughness obtained for SiC-30 wt% TaC composite. A slight decrement in the hardness of composites with increased the TaC content from 10 to 30 wt%. A maximum hardness of 25.75 GPa obtained for SiC-10 wt% TaC composites.

(c) Mixed mode of fracture i.e. intergranular and transgranular fracture occur for the sintered SiC-TaC composites.

(d) When eroded by SiC particle, the erosion rate decreased with the increase in TaC content. The maximum erosion is observed for SiC-10 wt% TaC composites, while it is minimum for SiC-30 wt% TaC composite. The erosion rate increased with increase in temperature to 400^{o}C.

(e) The worn surfaces reveal increased pull-out of grains when composites are eroded at 400^{o}C compared to ambient temperature.

CHAPTER 7

SCOPE FOR FUTURE WORK

1. The present study deals with the erosion at ambient and at 400°C temperature condition. Further experimentation can be done to understand the effect of high temperature (800-1000°C) on the performance of erosion.

2. The size of the erodent particles was 45-75μm size SiC powder in this study. We can also varied the erodent particle size to understand the effect of particle size on erosion for further studies.

3. The erosion test was performed only at normal angle of impingement in this study. For further studies we can also varied the angle of impingement like 30° and 60°.

4. Effect of various other erodent particles other than silicon carbide powder can be carried out to do the comparative study between different erodent particles on erosion performance.

5. Effect of parameters like impact velocity, discharge rate etc. on the erosion performance can also be studied.

6. Since in present work we have restricted only high temperature erosion test, future work may be extended to sliding wear test at higher temperatures and also cavitation and slurry erosion test.

CHAPTER 8

REFERENCES

1. F. F. Lange, “Hot-pressing behaviour of silicon carbide powders with additions of aluminium oxide.” J. Mater. Sci. 10 (1975) 314-320.
2. N. P. Padture, “In situ-toughened silicon carbide.” J. Am. Ceram. Soc. 77 (1994) 519-523.
3. G. Roewer1, U. Herzog, K. Trommer, E. Miiller, S. Friihauf, “Silicon carbide- a survey of synthetic approaches, properties and applications.” Struct. Bond. 101 (2002) 59-135.
4. X. Dong, S. Jahanmir, L. K. Ives, “Wear transition diagram for silicon carbide.” Tribo. Int.. 28 (1995) 559-572.
5. D. C. Cranmer, “Friction and wear properties of monolithic silicon-based ceramics.” J. Mater. Sci. 20 (1985) 2029-2037.
6. K. H. Z. Gahr, R. Blattner, D. H. Hwang, K. Pohlmann, “Micro and micro-tribological properties of SiC ceramics in sliding contact.” Wear 250 (2001) 299-310.
7. V. S. R. Murthy, H. Kobayashi, S. Tsurekawa, N. Tamari, T. Watanabe, K. Kato, “Influence of humidity and doping elements on the friction and wear of SiC in unlubricated sliding.” Tribo. Int. 37 (2004) 353-364.
8. Y. Wang, S. M. Hsu, “Wear and wear transition mechanisms of ceramics.” Wear 195 (1996) 112-122.
9. P. Anderson, A. Blomberg, “Instability in the tribochemical wear of silicon carbide in unlubricated sliding contacts.” Wear 174 (1994) 1-7.
10. S. J. Cho, C. D. Um, S. S. Kim, “Wear and wear transition in silicon carbide ceramics during sliding.” J. Am. Ceram Soc. 79 (1996) 1247-1251.
11. O. B. Lopez, A. L. Ortiz, F. Guiberteau, N. P. Padture, “Sliding-wear-resistant liquid-phase-sintered SiC processed using α-SiC starting powder.” J. Am. Ceram. Soc. 90 (2007) 541-545.

12. O. B. Lopez, A. L. Ortiz, F. Guiberteau, N. P. Padture, “Effect of microstructure on sliding-wear properties of liquid-phase-sintered α-SiC.” J. Am. Ceram. Soc. 88 (2005) 2159-2163.
13. O. B. Lopez, A. L. Ortiz, F. Guiberteau, N. P. Padture, “Microstructural design of sliding-wear-resistant liquid-phase-sintered SiC: An overview.” J. Eur. Ceram. Soc. 27 (2007) 3351-3357.
14. B. V. Manoj Kumar, Y. W. Kim, D. S. Lim, W. S. Seo, “Influence of small amount of sintering additives on unlubricated sliding wear properties of SiC ceramics.” Ceram. Intl. 37 (2011) 3509-3608.
15. J. L. Routbort, R. O. Scattergood, A. P. Turner, “The erosion of reaction-bonded SiC.” Wear 59 (1980) 363-375.
16. S. M. Weiderhorn, B. J. Hockey, “Effect of material parameters on the erosion resistance of brittle materials.” J. Mater. Sci., 18 (1983) 766-780.
17. D. F . Wang, J. H. She, Z. Y. Ma, “Effect of microstructure on erosive wear behaviour of SiC ceramics.” Wear 180 (1995) 35-41.
18. J. L. Routbort, R. O. Scattergood, “Anomalous solid particle erosion rate of hot pressed silicon carbide.” J. Am. Ceram. Soc., 63 (1980) 593-595.
19. J. J. Kim, S. K. Park, “Solid particle erosion of SiC and SiC-TiB_2 composite hot-pressed with Y_2O_3.” Wear 222 (1998) 114-119.
20. D. Jianxin, L. Lili, D. Mingwei, “Erosion wear behaviours of SiC/(W,Ti)C laminated ceramic nozzles in dry sand blasting processes.” Mater. Sci, Engg A444 (2007) 120-129.
21. Y.W. Kim, Y.Il Lee,,M Mitomo,, H.J Choi, J..G Lee, “Fabrication and Mechanical Properties of Silicon Carbide-Silicon Nitride Composites with Oxynitride Glass.” J. Am. Ceram. Soc. 82 (1999) 1058-1060.
22. Y. W. Kim, S. G. Lee, Y.Il Lee, “Pressureless sintering of SiC-TiC composites with improved fracture toughness.” J. Mater. Sci., 35 (2000) 5569 – 5574.
23. B. Basu, M. Kalin “ Tribology of ceramics and composites.” First ed., John Wiley & Sons, New Jersy, Am. Cer. Soc. (2011) 18–38.
24. W. Yi, X. Yongdong, W. Yiguang, C. Laifei, and Z. Litong, “Effects of TaC addition on the ablation resistance of C / SiC.” Mater. Lett.64 [19] (2010) 2068–2071.

25. D. Chen, X. F. Zhang, and R. O. Ritchie, “Effects of Grain-Boundary Structure on the Strength, Toughness, and Cyclic-Fatigue Properties of a Monolithic Silicon Carbide.” J. Am. Ceram. Soc., 83 [8] (2000) 2079-2081.
26. G. Rixecker, I. Wiedmann, A. Rosinus, and F. Aldinger, “High-Temperature Effect in the Fracture Mechanical Behavior of Silicon Carbide Liquid-Phase Sintered with AlN-Y_2O_3 Additives.” J. Eur. Ceram. Soc., 21 (200) 1013-1019.
27. S. G. Lee, Y. W. Kim, and M. Mitomo, “Relationship Between Microstructure and Fracture Toughness of Toughened Silicon Carbide Ceramics.” J. Am. Ceram. Soc., 84 (2001) 1347-1353.
28. Y. W. Kim, M. Mitomo, T. Nishimura, High-temperature strength of liquid-phase-sintered SiC with AlN and RE_2O_3 (RE: Y, Yb), J. Am. Ceram. Soc. 85 (2002) 1007-1009.
29. R. Yuan, J. J. Kruzic, X. F. Zhang, L. C. De Jonghe, and R. O. Ritchie, “Ambient to High-Temperature Fracture Toughness and Cyclic Fatigue Behavior in Al-Containing Silicon Carbide Ceramics.” Acta. Mater., 51 (2003) 6477-6491.
30. M. Suárez, A. Fernández, “Challenges and opportunities for Spark Plasma Sintering: A key technology for a New Generation of Materials.” Wear 10 (2010) 5772/53706.
31. B. Basu, “Some fundamentals on Spark Plasma Sintering as a processing tool to fabricate Biomaterials.”, Am. Cer. Soc.,New Jersy (2011) 38-42.
32. L. Liu, F. Ye, Y. Zhou,“New route to densify tantalum carbide at 1400 ◦C by spark plasma sintering.” Mater. Sci. Eng. A 528 (2011) 4710-4714.
33. L. Liu, F. Ye, Z. Zhang, and Y. Zhou, “Microstructure and mechanical properties of the spark plasma sintered TaC / SiC composites.” Mater. Sci. Eng. A 529 (2011) 479–484.
34. M. D. Unlu, G. Goller, O. Yucel, and F. C. Sahin, “The Spark Plasma Sintering of Silicon Carbide Ceramics Using Alumina.” 125[2] (2014) 257–259.
35. A. H. Rashed, “Properties and Characteristics of Silicon carbide.” (2002) 3-17
36. W.D. Kingery et al, “Introduction to Ceramics”, 2nd ed., Wiley, New York, (1976) 63.
37. http://accuratus.com/pdf/sicprops.pdf
38. R. Gerhardt, Properties and Applications of Silicon Carbide (2011) 195-231.
39. https://en.wikipedia.org/wiki/Silicon_carbide

40. H. Yeom, Y. Kim, and K. Joo, “Electrical , thermal and mechanical properties of silicon carbide – silicon nitride composites sintered with yttria and scandia.” J. Eur. Ceram. Soc., vol. 35[1] (2015) 77–86.
41. C. Zhang, X. Yao, Y. Li, H. Liang, J. Chen, and J. Zhang, “Effect of AlN addition on the thermal conductivity of pressureless sintered SiC ceramics.” Ceram. Int.41[7] (2015) 9107–9114.
42. A. Motealleh, A. L. Ortiz, O. Borrero-lópez, and F. Guiberteau, “Effect of hexagonal-BN additions on the sliding-wear resistance of fine-grained α -SiC densified with $Y_3Al_5O_{12}$ liquid phase by spark-plasma sintering.” J. Eur. Ceram. Soc. 34 [3] (2014) 565–574.
43. F. Cinar, B. Apak, I. Akin, H. E. Kanbur, D. H. Genckan, A. Turan, G. Goller, and O. Yucel, “Spark plasma sintering of B_4C - SiC composites.” Solid State Sci. 14[11,12] (2012) 1660–1663.
44. A. Vande Put, J. P. Laval, S. Valette, and G. Trolliard, “Role of boron on the Spark Plasma Sintering of an α -SiC powder.” Wear 28 (2008) 1881–1890.
45. M. S. Krupa, N. D. Kumar, R. S. Kumar, P. Chakravarthy, and K. Venkateswarlu, “Effect of zirconium diboride addition on the properties of silicon carbide composites.” Ceram. Int., 39 [8] (2013) 9567–9574.
46. Y. Luo, S. Li, W. Pan, and L. Li, “Fabrication and mechanical evaluation of SiC – TiC nanocomposites by SPS.” Wear 58 (2003) 150–153.
47. S. Kumar, B. V. Manoj, K. Lim, Y. Kim, and S. K. Nath, “Erosion behavior of SiC – WC composites.” Ceram. Int., 40 [5] (2014) 6829–6839.
48. N. Miyazaki, "Solid particle erosion of composite materials : A critical review.” 356 (2015) 254-259.
49. H. C. Meng and K. C. Ludema, “Wear models and predictive.” 183 (1995) 443–457.
50. J. Stokes, Thermal spraying 2008 retrieved from http://www.slideshare.net/varunteja7330/mi-291-chapter-4-learning-from-failure
51. Z. Feng and A. Ball, “The erosion of four materials using seven erodents — towards an understanding.” 233-235 (1999) 674–684.
52. P.H. Shipway, I.M. Hutchings, “The ro1e of particle properties in the erosion of brittle materials.” 193 (1996) 105–113.
53. G. Sundararajan, “Solid particle erosion behaviour of metallic materials at room and elevated temperatures.” 30 [5] (1997) 339–359.

54. Brown R., Kosco S. and Zun E.J. “Solid particle erosion of composite materials.” Wear 88 (1983) 181.
55. Levy A.V. and Chik P. “Solid particle erosion on different metallic materials.” Wear 89 (1983) 151.
56. Montgomery J.E. and Clarke J.M. SAE Summer Meetings, “ Erosion of metallic materials at elevated temperature.” 538A (1962).
57. J.L. Routbout and R.O. Scattergood, “Anomalous solid particle erosion rate of hot pressed silicon carbide.” J.Am. Cer. Soc. 63 (1981) 593.
58. I. Kleis and P. Kulu, “Solid particle erosion: occurence, prediction and control.” 12 (2008) 206.
59. H. Conrad and A.V.Levy, “Erosion of ceramics, in corrosion erosion-wear of materials at elevated temperature.” Wear 118 (1987) 77-94.
60. J.E.Ritter, L.Rosenfeld and K.Jakns, “Erosion and strength degradation in alumina.” Wear 111 (1986) 335-346.
61. F. Object, D. By, S. Ball, and E. Temperatures, "In a SiC / SiC ceramic matrix composite at ambient condition.” 254 (2008) 356-359.
62. X. Li, H. Ding, Z. Huang, M. Fang, and B. Liu, “Solid particle erosion-wear behavior of SiC – Si_3N_4 composite ceramic at elevated temperature.” Ceram. Int. 40 [10] (2014) 16201–16207.
63. G. Amirthan, A. Udayakumar, V. V. B. Prasad, and M. Balasubramanian, “Solid particle erosion studies on biomorphic Si / SiC ceramic composites.” Wear 268 (2010) 145–152.
64. G. R. Anstis, P. Chantikul, B. R. Lawn, and D. B. Marshall, “A critical evaluatuion of indentation techniques for measuring toughness: Part II”, J. Am. Cer. Soc.64 (1981) 533-538.